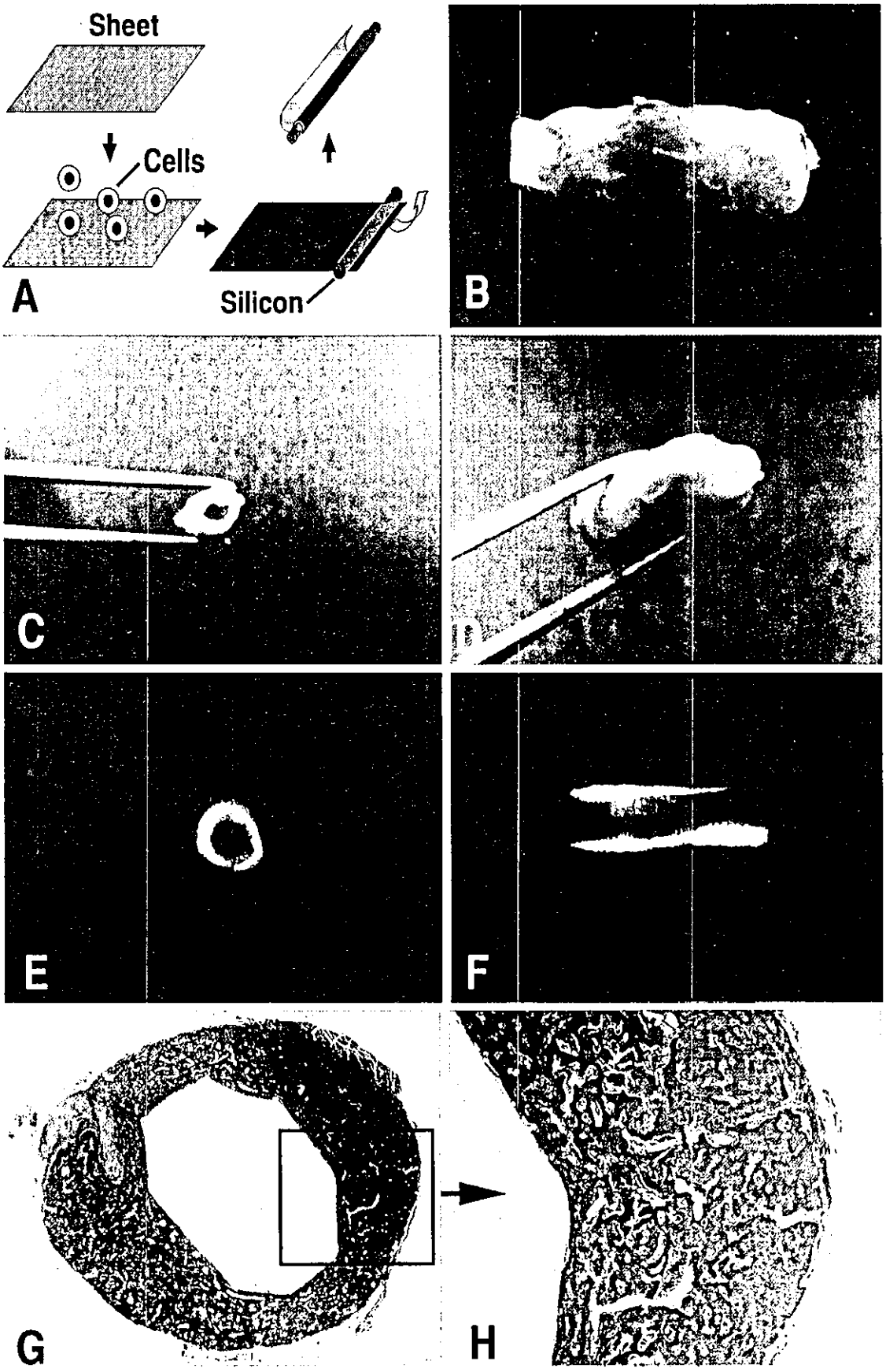

Fig. 8A–H Cylinder-shaped bone formation. **A** Protocol. **B** Solid bone formation around the silicone core after 4 weeks of subcutaneous tissue culture. Macroscopic views (**C, D**) and radiographs (**E** axial view, **F** longitudinal view) of a cylinder of bone after removal of the silicone core. **G** Histological view of a cross section. **H** Higher magnification of **G**. B ×1.4, C ×1, D ×1.4, E, F ×1, G ×6, H ×40

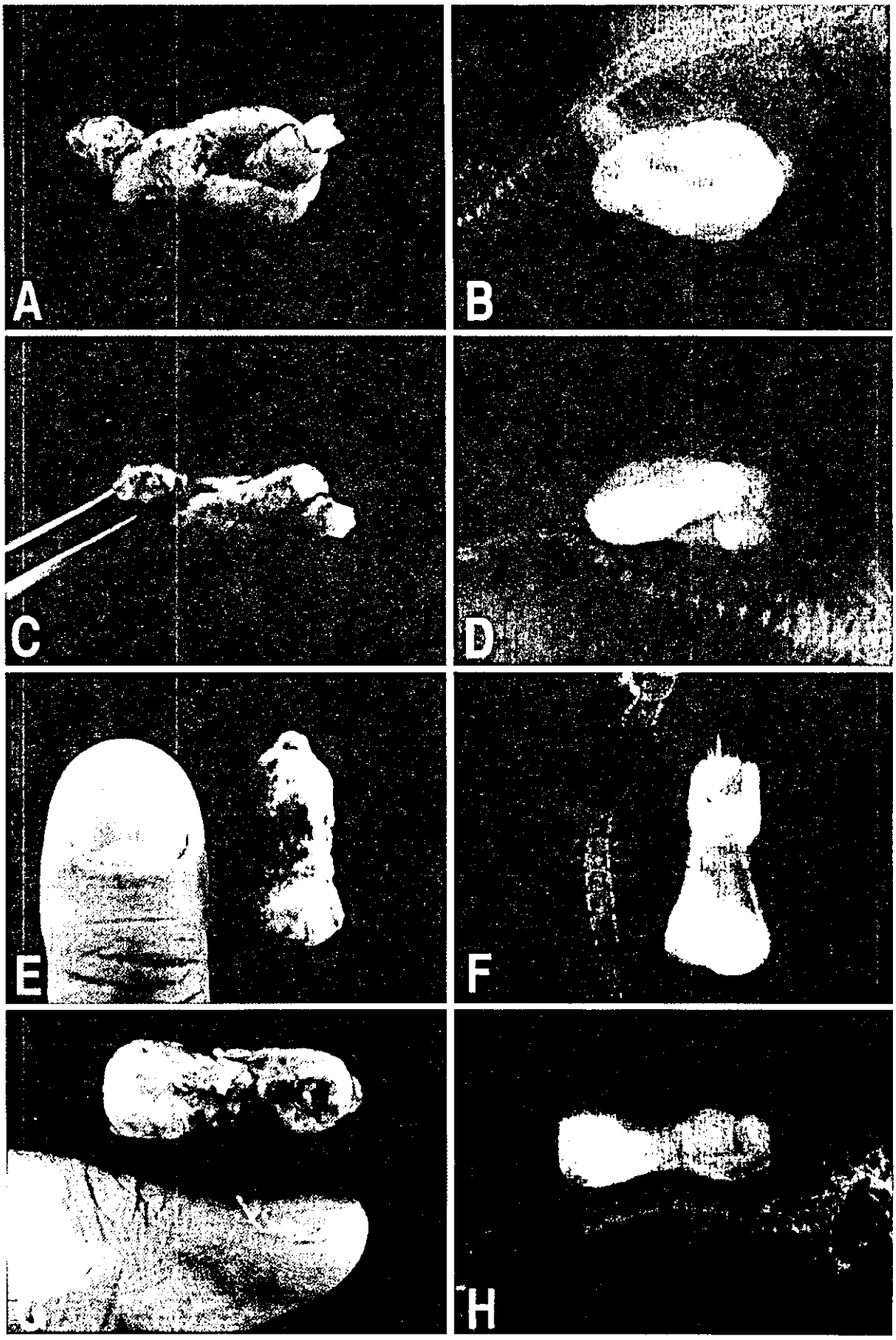

Fig. 9A–H Generation of a bone knot and phalanx-like bone. **A–D** Bone knot. Bone formed in the predesigned knotted PLGA/COL sheet. **A, C** Macroscopic view of a bone knot. **B, D** Radiographs of the bone knot in mice. **E–H** Phalanx-like bone. **E, G** Macroscopic view of the bone generated (with thumb of K.T. for reference). **F, H** Radiographs of the phalanx-like bone in mice. **A–D** ×1.3, **E–H** ×1.1

the synthetic fiber surface (Fig. 5A). The cells contained extensive dilated rough endoplasmic reticulum in their cytoplasm (Fig. 5B), thereby demonstrating the high affinity between the cells and collagen and the active protein-synthesizing capacity of the cells on the scaffold.

Implantation of laminated collagen hybrid PLGA sheets with KUSA-A1 cells for calvarial defects

We investigated whether calvarial defects were restored by the implantation of laminated collagen hybrid PLGA sheets with KUSA-A1 cells. No bridging of the cranial defects with new bone was observed at 4 weeks or at 8 weeks in mice, either in the sham-operated group or in the sheet alone group (n=10). The healing response in the control groups consisted of only a thin layer of connective tissue spanning the defects. Because of the scaffold remnants, the connective tissue was thicker in the defects treated with sheets alone than in the sham-operated group. By contrast, implantation of the hybrid PLGA sheet with KUSA-A1 cells over the calvarial defects resulted in closure of the defects with newly synthesized bone within 4 weeks in 10 out of 10 trials (Fig. 6). To determine the contribution of the implanted cells to osteogenesis, we labeled the implanted cells with β-galactosidase. The percentage of implanted cells was 96% in the generated bone, implying that most of the osteoblasts were derived from the donor cells. The thickness of the generated bone was variable and seemed to be related to the numbers of sheets. The scaffolds persisted at 4 weeks but had been completely absorbed at 8 weeks. The synthesized bone contained many vascular channels, and vascular endothelial cells were positive when immunohistochemically stained with Factor VIII antibody at 4 weeks. The newly formed bone contained a more prominent marrow space at 8 weeks. Bone healing was monitored radiographically at designated times after surgery (Fig. 7); the results showed a gradual increase in newly formed bone in the calvarial defects, and complete healing at 8 weeks.

Custom-shaped osteogenesis with PLGA/COL sheets

Since cylinder-shaped scaffolds are more suitable for segmental long bone defects, the cell-seeded sheets were rolled up around a hollow silicone rod (3 mm in diameter) immediately before implantation into subcutaneous tissue. After 4 weeks of cultivation in vivo, cylinder-shaped bone had formed (Fig. 8). Its outer circumference was covered with a fibrous layer, and ubiquitous vascular channels were connected to it. We then attempted to produce bone of more complex shapes (Fig. 9). The rolled sheets were knotted and transplanted into subcutaneous tissue, and uniquely shaped knots of bone were created. The cell-seeded sheets wrapped around silicone rubber blocks conformed well to the shape of the distal phalanx when removed from the mouse after 4 weeks.

Discussion

The shape of the sheets used in this study was not planned in advance. However, the sheets could easily be molded into desired shapes, such as a cylinder, knot, and phalanx. Thickness and shape could be adjusted by simply laminating, lapping, curling, or rolling the sheet, implying that almost any desired shape of bone can be produced with the sheets.

Up-regulation of cell adhesiveness by hybridization of collagen microsponge to hydrophobic sheets

Cells find it difficult to adhere to hydrophobic scaffolds, but hybridization of such scaffolds with collagen microsponges increases their cell adhesiveness. We have previously reported a novel three-dimensional porous scaffold hybridizing synthetic PLGA (Ochi et al. 2003) and naturally derived collagen for cartilage tissue engineering (Chen et al. 2000, 2001a). Osteoprogenitor cells can be readily processed into three-dimensional porous structures with desired pore morphological features that fit the defect, prior to surgery. However, cell seeding becomes more difficult as the thickness of the scaffold increases. Cell density and glycosaminoglycan content have been found to decrease with thickness in cartilage tissue engineering (Freed et al. 1994). Introduction of a novel PLGA-hybrid sheet with a thin planar sheet structure greatly improves cell seeding and even cell distribution. Since cell adhesion to the collagen microsponge in the opening of the PLGA is specific and rapid, this adhesion may result in transmission of "adhesive" signals that are important for the maintenance and/or commitment of marrow-derived stromal cells, such as osteoblasts and chondrocytes. This novel hybrid sheet shows a high degree of cell adhesion capacity and a more even cell distribution than we had expected.

Validity of the PLGA/COL hybrid sheet as a scaffold for bone tissue engineering

Biomaterials are essential for bone tissue engineering, and whether permanent or biodegradable, naturally occurring or synthetic, they must be biocompatible and ideally should be osteoinductive and osteoconductive (Urist 1965; Thomson et al. 1995). We have employed a PLGA/COL hybrid, one of the most promising scaffolds for osteogenesis. High-molecular weight molecules, such as poly(lactic acid) and poly(glycolic acid) (Laurencin et al. 1996; Gopferich et al. 1999), and inorganic materials, such as ceramics (Ohgushi et al. 1996), hydroxyapatite (Freed et al. 1999), and β-tricalcium phosphate (TCP), have been evaluated as scaffolds for osteogenesis. Hydroxyapatite and TCP efficiently conduct osteoprogenitor cells into themselves and become highly integrated with adjoining native bone (Osborn and Newesely 1980; Ohgushi et al. 1990), i.e., they have excellent osteocon-

ductivity and osseointegration properties. However, they do not induce osteogenic differentiation, i.e., they lack osteoinductivity. Moreover, problems arise associated with their slow biodegradability and their association with inflammation because of immunologic reactions.

Further modification of PLGA/COL sheets for bone tissue engineering

To circumvent these limitations, natural or synthetic materials and composite scaffolds based on poly(lactic acid), poly(glycolic acid), and their co-polymer, PLGA, have been developed to increase biodegradability (Ishaug et al. 1997; Ishaug-Riley et al. 1998) and decrease immunological reactions (Mikos et al. 1998). These synthetic polymers are mechanically stronger (Boyan et al. 1999) than naturally derived polymers, such as collagen, and the scaffold can be used either alone, in combination with osteoinductive growth factors, or with osteoconductive inorganic materials (Chen et al. 2001b; Kikuchi et al. 2002). Growth factors, such as bone morphogenetic proteins (Lane et al. 1999; Oldham et al. 2000; Peter et al. 2000) and vascular endothelial growth factor (Murphy et al. 2000; Tabata et al. 2000), can be incorporated into these synthetic polymers, and small hydroxyapatite particles can also be coated onto the polymers. Thus, the PLGA/COL hybrid sheet can be endowed with osteoinductivity and osteoconductivity to shorten the osteogenesis period after implantation and to obtain mechanical strength with plasticity. However, even after the addition of hydroxyapatite, the mechanical strength of the scaffold may be insufficient to maintain its original shape when the scaffold is used to treat long bone defects, and greater strength may be required to resist excessive mechanical overload or to support body weight. There is also concern that the acidic milieu associated with PLGA degradation may be toxic to cells and may induce inflammation (Bostman 1991; Wake et al. 1998), but we have found no evidence of such adverse reactions in our study.

Synthetic polymers are currently used for a number of orthopedic devices, including suture anchors and interference screws. Collagraft (Zimmer, Warsaw, Ind.), a composite of porous calcium phosphate granules and bovine-derived fibrillar collagen for bone regeneration (Cornell et al. 1991), was approved by the US Food and Drug Administration (FDA) in 1993 (Naughton 2002). Our hybrid sheet also consists of matrices that have been approved by the FDA. Some tissue-engineered skin replacement products are on the market, and the technology of tissue engineering for sheet materials is well-established. The scaffold used in this study retains large numbers of osteoprogenitors or osteoblasts derived from bone marrow, and because of its flexibility, assembles them into tissue of the desired shape in mice. The hybrid sheet is expected to become a useful scaffold for bone tissue engineering, and by taking advantage of its unique sheet form, it may be applicable elsewhere, such as in the regeneration of skin, blood vessels, ligaments, and periosteum, in addition to bone tissue engineering.

Acknowledgements We sincerely thank Y. Takeda and S. Matsumoto for support throughout the work, and N. Hida, T. Inomata, Y. Hashimoto, and Y. Nakamura for providing expert technical assistance.

References

Aronow MA, Gerstenfeld LC, Owen TA, Tassinari MS, Stein GS, Lian JB (1990) Factors that promote progressive development of the osteoblast phenotype in cultured fetal rat calvaria cells. J Cell Physiol 143:213–221

Bauer TW, Muschler GF (2000) Bone graft materials. An overview of the basic science. Clin Orthop 371:10–27

Bostman OM (1991) Osteolytic changes accompanying degradation of absorbable fracture fixation implants. J Bone Joint Surg Br 73:679–682

Boyan BD, Lohmann CH, Romero J, Schwartz Z (1999) Bone and cartilage tissue engineering. Clin Plast Surg 26:629–645

Chen G, Ushida T, Tateishi T (2000) A biodegradable hybrid sponge nested with collagen microsponges. J Biomed Mater Res 51:273–279

Chen G, Ushida T, Tateishi T (2001a) Poly(DL-lactic-co-glycolic acid) sponge hybridized with collagen microsponges and deposited apatite particulates. J Biomed Mater Res 57:8–14

Chen G, Ushida T, Tateishi T (2001b) Preparation of poly(L-lactic acid) and poly(DL-lactic-co-glycolic acid) foams by use of ice microparticulates. Biomaterials 22:2563–2567

Chen G, Sato T, Ushida T, Hirochika R, Tateishi T (2003) Redifferentiation of dedifferentiated bovine chondrocytes when cultured in vitro in a PLGA-collagen hybrid mesh. FEBS Lett 542:95–99

Chicurel ME, Chen CS, Ingber DE (1998) Cellular control lies in the balance of forces. Curr Opin Cell Biol 10:232–239

Cornell CN, Lane JM, Chapman M, Merkow R, Seligson D, Henry S, Gustilo R, Vincent K (1991) Multicenter trial of Collagraft as bone graft substitute. J Orthop Trauma 5:1–8

Crane GM, Ishaug SL, Mikos AG (1995) Bone tissue engineering. Nat Med 1:1322–1324

Freed LE, Grande DA, Lingbin Z, Emmanual J, Marquis JC, Langer R (1994) Joint resurfacing using allograft chondrocytes and synthetic biodegradable polymer scaffolds. J Biomed Mater Res 28:891–899

Freed LE, Martin I, Vunjak-Novakovic G (1999) Frontiers in tissue engineering. In vitro modulation of chondrogenesis. Clin Orthop 367 (Suppl):S46–S58

Friedenstein AJ (1976) Precursor cells of mechanocytes. Int Rev Cytol 47:327–359

Glowacki J, Mulliken JB (1985) Demineralized bone implants. Clin Plast Surg 12:233–241

Gojo S, Gojo N, Takeda Y, Mori T, Abe H, Kyo S, Hata J, Umezawa A (2003) In vivo cardiovasculogenesis by direct injection of isolated adult mesenchymal stem cells. Exp Cell Res 288:51–59

Gopferich A, Peter SJ, Lucke A, Lu L, Mikos AG (1999) Modulation of marrow stromal cell function using poly(D,L-lactic acid)-block-poly(ethylene glycol)-monomethyl ether surfaces J Biomed Mater Res 46:390–398

Haynesworth SE, Goshima J, Goldberg VM, Caplan AI (1992) Characterization of cells with osteogenic potential from human marrow. Bone 13:81–88

Ishaug SL, Crane GM, Miller MJ, Yasko AW, Yaszemski MJ, Mikos AG (1997) Bone formation by three-dimensional stromal osteoblast culture in biodegradable polymer scaffolds. J Biomed Mater Res 36:17–28

Ishaug-Riley SL, Crane-Kruger GM, Yaszemski MJ, Mikos AG (1998) Three-dimensional culture of rat calvarial osteoblasts in porous biodegradable polymers. Biomaterials 19:1405–1412

Kikuchi M, Koyama Y, Takakuda K, Miyairi H, Shirahama N, Tanaka J (2002) In vitro change in mechanical strength of beta-tricalcium phosphate/copolymerized poly-L-lactide composites and their application for guided bone regeneration. J Biomed Mater Res 62:265–272

Kohyama J, Abe H, Shimazaki T, Koizumi A, Nakashima K, Gojo S, Taga T, Okano H, Hata J, Umezawa A (2001) Brain from bone: efficient meta-differentiation of marrow stroma-derived mature osteoblasts to neurons with Noggin or a demethylating agent. Differentiation 68:235–244

Lane JM, Yasko AW, Tomin E, Cole BJ, Waller S, Browne M, Turek T, Gross J (1999) Bone marrow and recombinant human bone morphogenetic protein-2 in osseous repair. Clin Orthop 361:216–227

Langer R, Vacanti JP (1993) Tissue engineering. Science 260:920–926

Laurencin CT, El-Amin SF, Ibim SE, Willoughby DA, Attawia M, Allcock HR, Ambrosio AA (1996) A highly porous 3-dimensional polyphosphazene polymer matrix for skeletal tissue regeneration J Biomed Mater Res 30:133–138

Makino S, Fukuda K, Miyoshi S, Konishi F, Kodama H, Pan J, Sano M, Takahashi T, Hori S, Abe H, Hata J, Umezawa A, Ogawa S (1999) Cardiomyocytes can be generated from marrow stromal cells in vitro. J Clin Invest 103:697–705

Maniatopoulos C, Sodek J, Melcher AH (1988) Bone formation in vitro by stromal cells obtained from bone marrow of young adult rats. Cell Tissue Res 254:317–330

Mikos AG, McIntire LV, Anderson JM, Babensee JE (1998) Host response to tissue engineered devices. Adv Drug Deliv Rev 33:111–139

Minuth WW, Sittinger M, Kloth S (1998) Tissue engineering: generation of differentiated artificial tissues for biomedical applications. Cell Tissue Res 291:1–11

Murphy WL, Peters MC, Kohn DH, Mooney DJ (2000) Sustained release of vascular endothelial growth factor from mineralized poly(lactide-co-glycolide) scaffolds for tissue engineering. Biomaterials 21:2521–2527

Naughton GK (2002) From lab bench to market: critical issues in tissue engineering. Ann N Y Acad Sci 961:372–385

Ochi K, Chen G, Ushida T, Gojo S, Segawa K, Tai H, Ueno K, Ohkawa H, Mori T, Yamaguchi A, Toyama Y, Hata J, Umezawa A (2003) Use of isolated mature osteoblasts in abundance acts as desired-shaped bone regeneration in combination with a modified poly-DL-lactic-co-glycolic acid (PLGA)-collagen sponge. J Cell Physiol 194:45–53

Ohgushi H, Okumura M, Tamai S, Shors EC, Caplan AI (1990) Marrow cell induced osteogenesis in porous hydroxyapatite and tricalcium phosphate: a comparative histomorphometric study of ectopic bone formation. J Biomed Mater Res 24:1563–1570

Ohgushi H, Dohi Y, Yoshikawa T, Tamai S, Tabata S, Okunaga K, Shibuya T (1996) Osteogenic differentiation of cultured marrow stromal stem cells on the surface of bioactive glass ceramics. J Biomed Mater Res 32:341–348

Oldham JB, Lu L, Zhu X, Porter BD, Hefferan TE, Larson DR, Currier BL, Mikos AG, Yaszemski MJ (2000) Biological activity of rhBMP-2 released from PLGA microspheres. J Biomech Eng 122:289–292

Osborn JF, Newesely H (1980) The material science of calcium phosphate ceramics. Biomaterials 1:108–111

Owen M, Friedenstein AJ (1988) Stromal stem cells: marrow-derived osteogenic precursors. Ciba Found Symp 136:42–60

Peter SJ, Lu L, Kim DJ, Stamatas GN, Miller MJ, Yaszemski MJ, Mikos AG (2000) Effects of transforming growth factor beta1 released from biodegradable polymer microparticles on marrow stromal osteoblasts cultured on poly(propylene fumarate) substrates. J Biomed Mater Res 50:452–462

Pitaru S, Kotev-Emeth S, Noff D, Kaffuler S, Savion N (1993) Effect of basic fibroblast growth factor on the growth and differentiation of adult stromal bone marrow cells: enhanced development of mineralized bone-like tissue in culture. J Bone Miner Res 8:919–929

Sato T, Chen G, Ushida T, Ishii T, Ochiai N, Tateishi T (2001) Tissue-engineered cartilage by in vivo culturing of chondrocytes in PLGA-collagen hybrid sponge. Mater Sci Eng C17:83–89

Tabata Y, Miyao M, Ozeki M, Ikada Y (2000) Controlled release of vascular endothelial growth factor by use of collagen hydrogels. J Biomater Sci Polym Ed 11:915–930

Thomson RC, Yaszemski MJ, Powers JM, Mikos AG (1995) Fabrication of biodegradable polymer scaffolds to engineer trabecular bone. J Biomater Sci Polym Ed 7:23–38

Umezawa A, Tachibana K, Harigaya K, Kusakari S, Kato S, Watanabe Y, Takano T (1991) Colony-stimulating factor 1 expression is down-regulated during the adipocyte differentiation of H-1/A marrow stromal cells and induced by cachectin/tumor necrosis factor. Mol Cell Biol 11:920–927

Umezawa A, Maruyama T, Segawa K, Shadduck RK, Waheed A, Hata J (1992) Multipotent marrow stromal cell line is able to induce hematopoiesis in vivo. J Cell Physiol 151:197–205

Urist MR (1965) Bone: formation by autoinduction. Science 150:893–899

Vunjak-Novakovic G, Obradovic B, Martin I, Bursac PM, Langer R, Freed LE (1998) Dynamic cell seeding of polymer scaffolds for cartilage tissue engineering. Biotechnol Prog 14:193–202

Wake MC, Gerecht PD, Lu L, Mikos AG (1998) Effects of biodegradable polymer particles on rat marrow-derived stromal osteoblasts in vitro. Biomaterials 19:1255–1268

Gene Therapy (2004) 11, 1475–1481

www.nature.com/gt

RESEARCH ARTICLE

Brain transplantation of genetically modified bone marrow stromal cells corrects CNS pathology and cognitive function in MPS VII mice

K Sakurai[1,2], S Iizuka[1], J-S Shen[1], X-L Meng[1], T Mori[4], A Umezawa[3], T Ohashi[1,2] and Y Eto[1,2]

[1]*Department of Gene Therapy, Institute of DNA Medicine;* [2]*Department of Pediatrics, The Jikei University School of Medicine, Tokyo, Japan;* [3]*Department of Reproductive Biology and Pathology, National Research Institute for Child Health and Development, Tokyo, Japan; and* [4]*Department of Pathology, Keio University School of Medicine, Tokyo, Japan*

Current therapies for lysosomal storage diseases (LSDs), enzyme replacement therapy and bone marrow transplantation are effective for visceral organ pathology of LSD, but their effectiveness for brain involvement in LSDs is still a subject of controversy. As an alternative approach, we transplanted genetically modified bone marrow stromal (BMS) cells to lateral ventricle of newborn mucopolysaccharidosis VII (MPS VII) mice. MPS VII is one of LSDs and caused by deficiency of beta-glucuronidase (GUSB), resulting in accumulation of glycosaminoglycans (GAGs) in brain. At 2 weeks after transplantation, the GUSB enzyme-positive cells were identified in olfactory bulb, striatum and cerebral cortex, and the enzymatic activities in various brain areas increased. The GAGs contents in brain were reduced to near normal level at 4 weeks after transplantation. Although GUSB activity declined to homozygous level after 8 weeks, the reduction of GAGs persisted for 16 weeks. Microscopic examination indicated that the lysosomal distention was not found in treated animal brain. Cognitive function in MPS VII animals as evaluated by Morris Water Maze test in treated mice showed a marked improvement over nontreated animals. Brain transplantation of genetically modified BMS cells appears to be a promising approach to treat diffuse CNS involvement of LSDs.
Gene Therapy (2004) **11,** 1475–1481. doi:10.1038/sj.gt.3302338; Published online 5 August 2004

Keywords: *bone marrow stromal cells; MPS VII; intraventricular transplantation; beta-glucuronidase; Morris Water Maze*

Introduction

Mucopolysaccharidosis type VII (MPS VII, Sly syndrome) is one of lysosomal storage diseases (LSDs) caused by deficiency of beta-glucuronidase (GUSB), resulting in progressive accumulation of undegraded glycosaminoglycans (GAGs) in various tissues including the brain.[1,2] A murine model of MPS VII is available and its clinical, biochemical and pathological features closely reflect those of human MPS VII.[3–5] Using this mouse model, various therapeutic approaches including enzyme replacement therapy,[6–8] bone marrow transplantation (BMT),[9–11] gene therapy[12–14] and cell therapy[15–17] have previously been attempted with varying degree of success. In case of enzyme replacement therapy, patients must continue to receive enzyme replacement in their whole life and the cost of recombinant enzyme is another big burden to patients. BMT results in high mortality and morbidity rate, especially at early infancy. In gene therapy, although AAV vectors appear to have a promise, it is still difficult to produce large amount of recombinant virus. The safety issue of lentivirus vector is another major concern for use of this virus vector to human. In cell therapy, although transplantation of neural stem cells or amniotic cells shows a great hope to treat CNS involvement in MPS VII, ethical and immunologic problems must be cleared.

Recent studies have demonstrated that the bone marrow stromal (BMS) cells have ability to differentiate into osteocytes, chondrocytes, adipocytes, muscle and also into neural cells,[18–22] and that the brain transplantation of BMS cells induces good clinical outcome in neurological diseases such as brain infarction[23] and LSD.[24] Patient's BMS cells could be harvested by a simple bone marrow aspiration and grow rapidly in culture, and autologous transplantation can overcome ethical and immunologic problems associated with transplantation of neural stem cells or amniotic cells. In the present study, we demonstrate that the intraventricular transplantation of BMS cells overexpressing GUSB in neonatal MPS VII mice corrects the CNS pathology and function in these mutant mice.

Correspondence: Dr T Ohashi, Department of Gene Therapy, Institute of DNA Medicine, The Jikei University School of Medicine, 3-25-8 Nishishinbashi, Minato-ku, Tokyo, Japan
Received 4 May 2004; accepted 22 June 2004; published online 5 August 2004

Results

Transduction of KUSA/A1 by MND/HBG

KUSA/A1, mouse bone marrow stromal cell, was transduced with human GUSB gene by retrovirus vector. The GUSB activity in transduced cell (KUSA/HBG) was increased from 5.9×10^1 to 1.9×10^6 nmol/h/mg. Histochemical staining of GUSB-bearing KUSA/HBG cells exhibited positive staining for GUSB, while parental

KUSA/A1 cells were negative for the staining (data not shown). These results are consistent with the data of enzymatic activity.

Distribution of GUSB activity in the brain after transplantation

At 2 and 8 weeks after transplantation, GUSB activities in the recipient brains were determined. Serial coronal sections of mouse brain as shown in Figure 1 were collected and GUSB activity was assayed quantitatively in each section. GUSB activity in all brain regions of treated MPS VII mice 2 weeks after transplantation was higher than in those of age-matched untreated MPS VII mice (Figure 1). GUSB activity of treated MPS VII mouse brain was approximately 50 times higher than that of untreated MPSVII mice in each section. This value corresponds to approximately 20% of heterozygote mouse level. At 8 weeks after transplantation, GUSB activity in treated mouse brain declined to homozygote mouse level.

Biochemical response of the brain in treated MPS VII mice

It has been known that the enzyme activity of other lysosomal enzymes such as α-galactosidase A (α-Gal) and hexosaminidase (Hex) are elevated in MPS VII mouse brain, and that the reduction of these enzymes by treatment is well correlated with therapeutic effect.[8–10] Thus, to monitor the therapeutic effect of cell transplantation, we assayed enzyme activities of α-Gal and Hex in the brain of mice at 2 weeks after transplantation. Activities of both enzymes in the treated mouse brain decreased to those of heterozygous mouse level (Figure 2a, b).

Histochemical detection of GUSB-positive cells in treated mouse brain

At 2 weeks after transplantation, we examined the survival and distribution of transplanted cells by GUSB histochemical analysis. In transplanted mice GUSB positive cells (red) were found not only in meninges and subventricular regions (Figure 3a) but also in

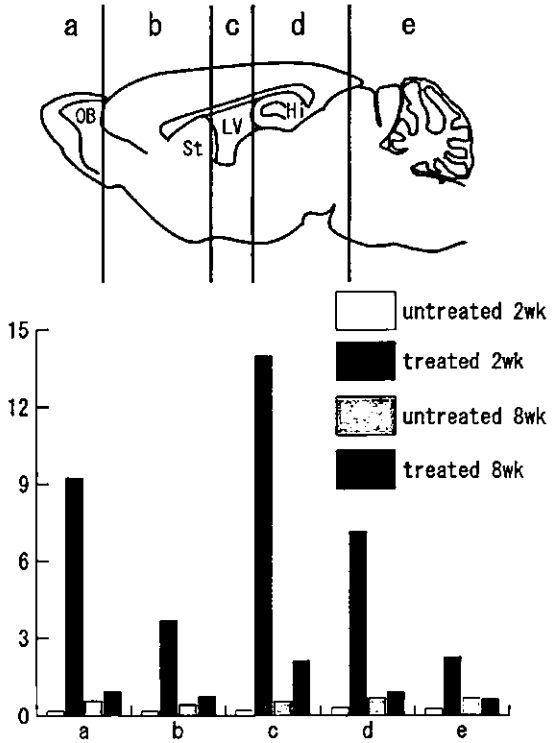

Figure 1 GUSB activity in various regions of the brain after transplantation. Average of GUSB activity in various regions of the brain of mice at 2 (n=2) and 8 (n=3) weeks after transplantation and age-matched untreated mutant mice. Mouse brains were divided into serial five coronal sections. The regions were defined by anatomical landmark: a, olfactory bulb; b, from end of olfactory bulb to beginning of striatum; c, striatum to the rostal edge of the hippocampus; d, hippocampus to colliculus and midbrain; e, cerebellum and brain stem. GUSB activity was expressed as nmol/h/mg protein.

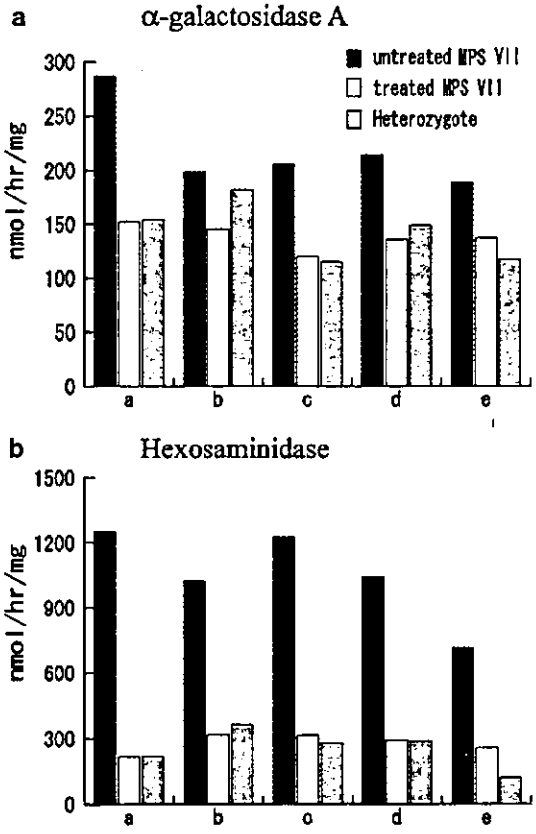

Figure 2 α-Galactosidase A (α-Gal) and hexosaminidase (Hex) activity in various brain regions of treated MPS VII mice. At 2 weeks after transplantation, average activities of α-Gal (a) and Hex (b) in the same tissues (n=2) as described in Figure 1. These enzymatic activities in the brain of treated MPS VII decreased to heterozygous level. These activities are expressed as nmol/h/mg protein.

Figure 3 Histochemical detection of GUSB-positive cells in treated mouse brain. Cryosection of the brain in treated MPS VII mice at 2 weeks after transplantation. The GUSB positive cells were detected in various regions, (a) subventricle, (b) cerebral cortex, and (c) olfactory bulb, of transplanted MPS VII mouse brain. (bar=200 μm).

cerebral cortex (Figure 3b) and olfactory bulb (Figure 3c), while GUSB-positive cells were not found in control untreated brain.

Correction of lysosomal distention in the brain of treated MPS VII mice

To evaluate lysosomal distention of MPS VII mouse brain, histopathological analysis was performed in variety of brain regions, such as cerebral cortex, olfactory bulb, and striatum at 4 weeks after transplantation (Figure 4). Profound lysosomal distention in neural cell was observed in age-matched untreated MPS VII mice (indicated by arrow, Figure 4a–c), while this was not observed in olfactory bulb (Figure 4d), striatum (Figure 4e) or cortex (Figure 4f) in treated MPS VII mouse brain. There was no lysosomal distension in the brain of the heterozygous mouse (data not shown).

Reduction in levels of GAGs in the brain of treated MPS VII mice

Levels of GAGs in the brain were determined in treated MPS VII mice at 4, 8, 16 weeks after transplantation (Table 1). In this study, we assayed amount of total chondroitin sulfate (T-CS) and hyaluronic acid (HA), which are known to accumulate in the MPS VII brain. At 4 weeks after transplantation, both of these two GAGs in treated MPS VII mice were reduced significantly as compared to age-matched untreated MPS VII mice (T-CS; $P=0.0012$, HA; $P=0.0002$ respectively). Although the enzymatic activity diminished to homozygous level 8 weeks after transplantation, a significant reduction (T-CS; $P=0.0071$, HA; $P=0.0001$) of GAGs in the brain of treated MPS VII mice persisted up to 16 weeks after treatment.

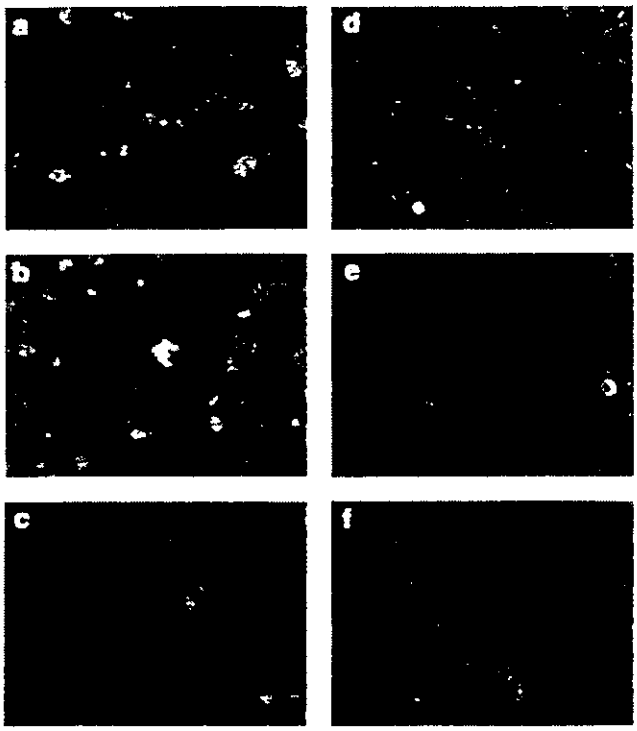

Figure 4 Correction of lysosomal distention in the brain of treated MPS VII mice. Pathological analysis of the MPS VII mouse brain. (a–c) Untreated MPS VII mouse brain. (d–f) Treated MPS VII mouse brain. (a and d) olfactory bulb, (b and e) striatum and (c and f) cerebral cortex of the mouse brain. Although there were many cells with lysosomal distention in the multiple brain regions of untreated MPS VII mice (a–c), all regions of treated MPS VII mouse brain 4 weeks after transplantation (d–f) have no lysosomal storage vacuoles. (bar = 40 μm).

Table 1 Reduction in levels of glycosaminoglycans (GAGs) in the brain of treated MPS VII mice

	Age (n)	*T-CS (μg/g wet-tissue)*	*HA (μg/g wet-tissue)*
Untreated	4 wk ($n=3$)	316.600 (±14.860)	87.967 (±2.835)
MPS VII	8 wk ($n=3$)	531.733 (±39.434)	82.667 (±4.447)
	16 wk ($n=3$)	523.067 (±32.452)	87.400 (±1.877)
Treated	4 wk ($n=4$)	131.975 (±21.276)*	34.275 (±3.95)**
MPS VII	8 wk ($n=3$)	255.167 (±15.048)*	34.900 (±2.757)**
	16 wk ($n=3$)	312.467 (±25.894)*	45.500 (±2.100)**
Normal	4 wk ($n=3$)	85.800 (±3.980)	24.467 (±1.110)
	8 wk ($n=3$)	182.400 (±8.228)	36.733 (±5.584)
	16 wk ($n=3$)	145.267 (±19.368)	44.967 (±5.109)

*$P<0.01$, **$P<0.001$.
Versus untreated MPS VII mice.
Total chondroitin sulfate (T-CS) and hyaluronic acid (HA) of GAGs were measured biochemically 4, 8 and 16 weeks after transplantation by HPLC methods. *Indicates significant reduction ($P<0.01$) *versus* age-matched untreated MPS VII mice. **Indicates significant reduction ($P<0.001$) *versus* age-matched untreated MPS VII mice.

Improvement of cognitive function with the Morris Water Maze (MWM) test

We performed the visible test before nonvisible test and there was no significant difference of normal mice and untreated MPS VII mice at 6 weeks old (data not shown). These data indicate that there is no significant difference of motor function between wild-type mouse and mutant mouse. At 6 weeks after transplantation, we performed the MWM to evaluate improvement of cognitive function by the treatment. Mice were adapted to the pool at the day before the acquisition phase. The acquisition phase: All of mice were trained from day 1 to day 5 to memorize the platform place. The probe test (Figure 5): The probe test was performed on day 6, immediately after the acquisition phase. The platform was removed and the amount of time spent in each quadrant was monitored. It is well known that normal mice spend longer time in target quadrant where the platform was placed at the acquisition phase than the mean of other three nontarget quadrants. Average of the time spent in the target quadrant by treated mice was 22.4 (s), whereas average of the time spent by untreated mice was 18.2 (s). Treated MPS VII mice spent significantly more time in the target quadrant than in the mean of other three nontarget quadrants ($P=0.0028$), whereas in untreated MPS VII mice the difference of time spent in the target quadrant and the mean of the other three nontarget quadrants was not statistically significant ($P=0.3201$).

Discussion

Current available therapies for LSDs are BMT and enzyme replacement therapy. However, both approaches have inherent problems. BMT has high mortality and morbidity rate and enzyme replacement therapy has economic problems and life-long infusion of enzyme

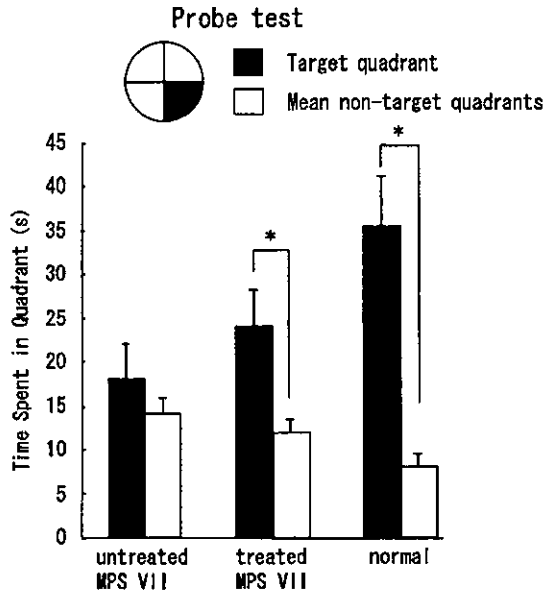

Figure 5 Improvement of cognitive function with the Morris Water Maze Test. The probe test was performed on day 6 immediately after the acquisition phase. After the platform was removed, the amount of time spent in each quadrant was monitored. Filled bars indicate the time spent in the target quadrant, and open bars indicate the average time spent in each of the three nontarget quadrants. Treated MPS VII mice and normal mice spent significantly more time in the target quadrant than in the other three nontarget quadrants ($P<0.001$), whereas in untreated MPS VII mice the difference of time spent in target quadrant and the other three nontarget quadrants was not statistically significant ($P=0.320$). Untreated MPS VII mice ($n=5$), treated MPS VII mice ($n=6$), normal mice ($n=5$).

replacement is required. Moreover, it is still controversial whether both approaches have a therapeutic effect for CNS involvement in the LSDs. To circumvent these problems, various approaches have been attempted to develop a new treatment for CNS involvement of LSDs, such as gene therapy and cell therapy. However, both approaches still have limitations. In gene therapy, although AAV vectors appear to have a promise, it is still difficult to produce large amount of recombinant virus. The safety issue of lentivirus vector is another major concern for use of this virus vector to human. In cell therapy, although transplantation of neural stem cells or amniotic cells shows a great hope to treat CNS involvement in MPS VII, ethical and immunologic problems must be cleared.

In the present study, we tested BMS cells as a vehicle to deliver the missing enzyme to wide region of the brain of LSD mouse model. The BMS cells have several advantages as compared to other stem/progenitor cells. First, the BMS cells are readily accessible from bone marrow and grow well *in vitro*. Second, the autologous transplantation overcomes the ethical and immunologic concerns. BMS cells have capability to differentiate into various neural cell lineages. We generated GUSB overexpressing BMS cell (KUSA/HBG) and KUSA/HBG was transplanted into lateral ventricle of newborn MPS VII mice. At 2 weeks after transplantation, expression of GUSB was observed in all of brain lesions. GUSB histochemical staining revealed that transplanted cells migrated to various brain regions not only ventricles also brain parenchyma, including cerebral cortex and olfactory bulb. Even though the number of transplanted cells in brain parenchyma was small, the pathological improvement is significant. Lysosomal storage in most of cells, such as endothelial cells, glial cells and neurons from various brain regions, was reduced. The amount of T-CS and HA, which was accumulated GAGs in MPS VII brain, was also reduced markedly.

To assess the functional improvement of the treated animals, we performed the MWM testThe MWM is known as test to evaluate cognitive functions. At 6 weeks after the transplantation, treated MPS VII mice spent significantly more time in the target quadrant than in the other three nontarget quadrants and the time spent in the target quadrant by treated MPS VII increased compared with by untreated MPS VII mice. Earlier report also demonstrated that the enzyme replacement therapy in neonatal period,[7] gene therapy using lentivirus vector[14] successfully restored brain function of MPS II mice. The expression of GUSB in the brain of treated animals 8 weeks after transplantation was markedly reduced. This relatively early reduction of GUSB activity in transplanted cells might be due to a mismatched allograft transplantation. KUSA/A1 cells are derived from C3H mouse, while MPS VII mice are C57BL/6 background. In addition, because KUSA/HBG expresses huge amount of human enzyme and the mouse immune system might recognize transplanted cell as a foreign cells. Thus, there is a possibility that transplanted cells were rejected by immunological mechanisms. Another possibility is that the transplanted cells underwent apoptosis from other unspecified mechanisms. We previously transplanted human neural stem cells into lateral ventricle of newborn MPS VII mice.[16] The human neural cells transduced with GUSB gene successfully corrected CNS pathology and restored enzyme levels, but grafted cells later underwent cell death by apoptosis mechanisms. The experiment is currently under way to understand the mechanism(s) for early death of KUSA/HBG cells in mouse brain. In the present study, although GUSB activity of treated mice 8 weeks after transplantation declined to those of untreated mice, interestingly, the restored GAGs contents in treated mouse brain were maintained up to 16 weeks after transplantation. Moreover the MWM showed that the brain function of treated mice still improved.

These results suggest that once MPS VII mice receive certain amount of GUSB cells in early stage, the brain function was maintained even after the considerable reduction of enzymatic activity. GAGs synthesis and GAGs turn over in adult MPS VII brain may be small so that GAGs do not re-accumulate. Large amount of GUSB may not be necessary for adult MPS VII brain after newborn brain treatment with GUSB.

Another question is what kinds of cell types transplanted cells differentiate into following brain transplantation. Previous reports have shown that the marrow stromal cells transplanted into the brain migrate to the parenchyma and differentiate into neural cells.[21,22] Number of KUSA/HBG cells in brain parenchyma was too small to perform double immunostaining, thus we performed another set of experiments. Briefly, KUSA/A1 cells were transduced by a LacZ expressing retrovirus vector and transplanted into striatum of adult C57BL/6 mice. After transplantation, frozen sections were made and double stained with anti-LacZ antibody and cell

type specific antibody, such as anti-NeuN for neurons, and anti-GFAP for astrocytes. Although a small number of LacZ positive cells expressed NeuN, majority of LacZ positive cells did not express any cell type specific makers (data not shown). These observations suggest that even if these cells have a migrating capacity in mouse brain, most of cells lost differentiation capability *in vivo*. We do not know the reason why our results differ from those of previous reports. However, for our purpose, transplanted cells do not necessarily differentiate into certain neural cells, such as neuron and glial cells. In another words, in order to treat the brain pathology of MPS VII mice, enzyme competent cell should migrate to various brain lesions and cross correct enzyme deficient neighboring cells.[25] In this regard, even if transplanted BMS cells did not differentiate into neural cells, BMS cell transplantation can correct the brain involvement of MPS VII. There are still some obstacles to be overcome to use BMS cell as a vehicle for treatment of brain involvement of LSDs. We transplanted BMS cells during neonatal period. However, it is quite rare that LSDs patients were diagnosed in this period. The development of newborn screening system for early detection of LSDs patients may overcome this problem. We do not know if BMS cell transplantation should have beneficial effect for the CNS involvement in MPS VII in later stage. Since a previous study has demonstrated that the BMS cell brain transplantation in Niemann–Pick disease mice at 3 weeks of age was effective for CNS involvement,[24] this may be the case for MPS VII as well. The transplantation of BMS cell into the brain in MPS mice at 3–4 weeks of age is underway.

In conclusion, we have demonstrated that the intraventricular transplantation of BMS cells overexpressing GUSB in neonatal MPS VII mice corrects the biochemical defects, CNS pathology and cognitive behavior in these mutant mice.

Materials and methods

Animals

Breeding pairs of (+/mps) were purchased form the Jackson Laboratory and bred in our institutional animal facility. Mutant mice (−/−) were identified by genetic analysis of DNA from mouse tail.[26] Enzymatic activity of tail was also measured as described below to confirm the diagnosis. Animals were maintained on a 12-h light/dark cycle and given a standard rodent chow.

BMS cell

Mouse BMS cell line, KUSA/A1, was established by limiting dilution of Dexter long-term cultures from C3H/He female mouse. The detailed methods and characters of this cell line were described previously.[20] This cell line is able to differentiate into osteoblasts and neural cells, including neurons, astrocytes and oligodendrocytes under specific conditions. This cell line was cultivated in DMEM/10% FCS at 37°C and 5% CO_2.

In vitro *retroviral transduction*

Full-length human GUSB cDNA (provided by Dr WS Sly of Saint Louis University) was cloned into *Eco*RI site of retrovirus vector plasmid pMNDXSN (provided by Dr DB Kohn of University Southern California).[27] The recombinant retrovirus expressing human GUSB was generated by transfection of this plasmid to PA317 packaging lines. The condition medium of packaging cells were collected and filtered through 0.45 μm filter. The resultant condition medium was added to ~50% confluent KUSA/A1 cells and incubated at 37°C for 2 h in the presence of polybrene (8 μg/ml). After incubation, the condition medium was removed and fresh medium (DMEM/10% FCS) was added. About 24 h later, the cells were selected with G418 (400 μg/ml) and resistant cells were pooled (KUSA/HBG). The GUSB activity in KUSA/HBG was assayed as described below to confirm successful transduction. Cytochemical analysis of GUSB was also performed.

Intraventricular transplantation of KUSA/HBG

KUSA/HBG was washed and harvested by 0.1% trypsin. The cells were resuspended in PBS and injected into the both lateral ventricles of mice within 48 h after birth using a 30G needle attached to a Hamilton syringe.[28] At this age, mutant mice do not exhibit any clinical and pathological symptoms. Thus, we expect maximized therapeutic effect. Injected volume of cell suspension was approximately 5 μl and the number of transplanted cells per mouse was from 1×10^5 to 1×10^6.

Histochemical/cytochemical analysis of GUSB

Transplanted mice were killed at 2 weeks after transplantation. Brain was removed and immediately embedded with OCT compound (Miles) and frozen in a liquid nitrogen bath. The samples were cut 10 μm sections by cryostat. The sections were fixed with chloral-formal-acetone fixative. The histochemical analysis of GUSB activity was performed using naphthol-AS-BI β-D-glucuronide as a substrate. The detail method of this staining was described elsewhere.[26] After hisitochemical staining of GUSB, sections were counterstained with 1% methyl green. The culture cells were fixed and stained with same method as stated above.

Lysosomal enzymes activities

Cells were washed briefly with PBS twice and harvested by 0.1% trypsin. After centrifugation, cell pellets were stocked at −80°C until assay. Cell pellets were resuspended in water and sonicated. The cell lysate was centrifuged at 14 000 *g* for 10 min at 4°C. The treated mice, age-matched mutant (−/−) and heterozygote (+/−) mice were killed at 2 and 8 weeks after transplantation. Harvested mouse brains were also stocked at −80°C until assay. To assess the distribution of transplanted cells, brain was cut into five serial coronal sections (Figure 1). To make tissue lysate, tissue was homogenized in water using a glass homogenizer. The homogenates were also centrifuged at 14 000 *g* for 10 min at 4°C and the resultant supernatant was used as enzyme source. The enzymatic activities of GUSB, α-Gal and Hex were measured fluorometrically using the artificial substrate, 4-methylumbelliferyl (4MU) β-D-glucuronide, 4MU α-D-galactopyranoside and 4MU *N*-acetyl-β-D-glucosaminide dihydrate (Sigma) respectively.[26,29,30] Protein concentration was determined by the BCA kit (Pierce) following the manufacture's instruction. Activity was expressed as nanomoles of 4-methylumbelliferone released per mg protein per hour.

Histopathological analysis of lysosomal distension

At 4 weeks after transplantation, treated mice, age-matched mutant and heterozygote mice were killed. Small blocks ($3 \times 3 \times 3$ mm^3) of various brain regions (olfactory bulb, cerebral cortex, and striatum) were immersed in 2% glutaraldehyde in PBS and fixed for 2–3 weeks. After fixation, the samples were embedded in Epon-araldite. Ultrathin sections (1.0 μm) were cut and were stained with toluidine blue to evaluate lysosomal distention.[5,26]

Analysis of GAG contents

Brain contents of T-CS and HA, which is substrate of GUSB, were measured by enzyme digestion and HPLC method.[31] The amount of T-CS and HA were expressed as μg/g wet tissue.

The MWM test

The MWM test was carried out at 6 weeks after transplantation. The acquisition phase and the probe test of the MWM test were performed as previously described.[32,33] The MWM test was slightly modified for this test. Briefly, the pool of a diameter 100 cm was filled 30 cm deep with water at 20°C. A transparent circular plexiglass platform 10 cm in a diameter was placed 1 cm below the surface of the water and 20 cm from the wall of the pool. The pool was designed as divided into four quadrants. The mice were released to the pool facing the wall at three points, four trials per a day were made for each mouse and the order of the releasing points was selected at random but all mice were followed the same order. If the mouse found the platform within 60 s, it was allowed to stay on the platform for 15 s. If the mouse could not find the platform within 60 s, it was guided to the platform by experimenter and it was allowed to stay on the platform for 15 s. All of the mouse traces were recorded by the over-head video camera. The acquisition phase of the test was performed for the 5 consecutive days (days 1–5). On day 6, the platform was removed and mice were released from the opposite side of the original platform place and the amount of time spent in each quadrant was monitored (the probe test).

Statistical analysis

A two-tailed Student's *t*-test was used for comparing the significance. The data are presented as mean ± s.e. *P*-value less than 0.05 was considered as significant.

Acknowledgements

We thank Drs DB Kohn (University of Southern California) and WS Sly (Saint Louis University School of Medicine) for kindly providing retrovirus vector and GUSB cDNA, respectively. We thank M Aoki and M Morimatsu of Laboratory Animal Center, The Jikei University School of Medicine, and H Maeda and H Fujita of Seikagaku Corporation for technical assistance. We also thank Dr SU Kim (University of British Columbia) for critical reviewing of this manuscript. This research was supported by the Bio-Venture Research Fund Project grant from the Ministry of Education, Science and Culture of Japan.

References

1 Neufeld EF, Muenzer J. The mucopolysaccharidosis. In: Scriver CR (ed). *In the Metabolic Basis of Inherited Disease*. McGraw-Hill Inc: New York, 1989, pp 3421–3452.
2 Sly WS *et al*. Beta glucuronidase deficiency: report of clinical, radiologic, and biochemical features of a new mucopolysaccharidosis. *J Pediatr* 1973; **82**: 249–257.
3 Birkenmeier EH *et al*. Murine mucopolysaccharidosis type VII. Characterization of a mouse with beta-glucuronidase deficiency. *J Clin Invest* 1989; **83**: 1258–1266.
4 Sands MS, Birkenmeier EH. A single-base-pair deletion in the beta-glucuronidase gene accounts for the phenotype of murine mucopolysaccharidosis type VII. *Proc Natl Acad Sci USA* 1993; **90**: 6567–6571.
5 Vogler C *et al*. A murine model of mucopolysaccharidosis VII. Gross and microscopic findings in beta-glucuronidase-deficient mice. *Am J Pathol* 1990; **136**: 207–217.
6 Vogler C *et al*. Enzyme replacement with recombinant beta-glucuronidase in the newborn mucopolysaccharidosis type VII mouse. *Pediatr Res* 1993; **34**: 837–840.
7 O'Connor LH *et al*. Enzyme replacement therapy for murine mucopolysaccharidosis type VII leads to improvements in behavior and auditory function. *J Clin Invest* 1998; **101**: 1394–1400.
8 Sands MS *et al*. Enzyme replacement therapy for murine mucopolysaccharidosis type VII. *J Clin Invest* 1994; **93**: 2324–2331.
9 Bastedo L *et al*. Behavioral consequences of bone marrow transplantation in the treatment of murine mucopolysaccharidosis type VII. *J Clin Invest* 1994; **94**: 1180–1186.
10 Sands MS *et al*. Treatment of murine mucopolysaccharidosis type VII by syngeneic bone marrow transplantation in neonates. *Lab Invest* 1993; **68**: 676–686.
11 Birkenmeier EH *et al*. Increased life span and correction of metabolic defects in murine mucopolysaccharidosis type VII after syngeneic bone marrow transplantation. *Blood* 1991; **78**: 3081–3092.
12 Frisella WA *et al*. Intracranial injection of recombinant adeno-associated virus improves cognitive function in a murine model of mucopolysaccharidosis type VII. *Mol Ther* 2001; **3**: 351–358.
13 Passini MA *et al*. Intraventricular brain injection of adeno-associated virus type 1 (AAV1) in neonatal mice results in complementary patterns of neuronal transduction to AAV2 and total long-term correction of storage lesions in the brains of beta-glucuronidase-deficient mice. *J Virol* 2003; **77**: 7034–7040.
14 Brooks AI *et al*. Functional correction of established central nervous system deficits in an animal model of lysosomal storage disease with feline immunodeficiency virus-based vectors. *Proc Natl Acad Sci USA* 2002; **99**: 6216–6221.
15 Snyder EY, Taylor RM, Wolfe JH. Neural progenitor cell engraftment corrects lysosomal storage throughout the MPS VII mouse brain. *Nature* 1995; **374**: 367–370.
16 Meng XL *et al*. Brain transplantation of genetically engineered human neural stem cells globally corrects brain lesions in the mucopolysaccharidosis type VII mouse. *J Neurosci Res* 2003; **74**: 266–277.
17 Kosuga M *et al*. Engraftment of genetically engineered amniotic epithelial cells corrects lysosomal storage in multiple areas of the brain in mucopolysaccharidosis type VII mice. *Mol Ther* 2001; **3**: 139–148.
18 Pittenger MF *et al*. Multilineage potential of adult human mesenchymal stem cells. *Science* 1999; **284**: 143–147.
19 Jiang Y *et al*. Pluripotency of mesenchymal stem cells derived from adult marrow. *Nature* 2002; **418**: 41–49.
20 Kohyama J *et al*. Brain from bone: efficient 'meta-differentiation' of marrow stroma-derived mature osteoblasts to neurons with Noggin or a demethylating agent. *Differentiation* 2001; **68**: 235–244.

21 Kopen GC, Prockop DJ, Phinney DG. Marrow stromal cells migrate throughout forebrain and cerebellum, and they differentiate into astrocytes after injection into neonatal mouse brains. *Proc Natl Acad Sci USA* 1999; **96**: 10711–10716.
22 Azizi SA *et al*. Engraftment and migration of human bone marrow stromal cells implanted in the brains of albino rats – similarities to astrocyte grafts. *Proc Natl Acad Sci USA* 1998; **95**: 3908–3913.
23 Zhao LR *et al*. Human bone marrow stem cells exhibit neural phenotypes and ameliorate neurological deficits after grafting into the ischemic brain of rats. *Exp Neurol* 2002; **174**: 11–20.
24 Jin HK *et al*. Intracerebral transplantation of mesenchymal stem cells into acid sphingomyelinase-deficient mice delays the onset of neurological abnormalities and extends their life span. *J Clin Invest* 2002; **109**: 1183–1191.
25 Taylor RM, Wolfe JH. Cross-correction of beta-glucuronidase deficiency by retroviral vector-mediated gene transfer. *Exp Cell Res* 1994; **214**: 606–613.
26 Wolfe JH, Sands MS. Murine mucopoluysaccharidosis type VII: a model system for somatic gene transfer of the central nervous system. In: Lowenstein PR (ed). *Protocols for Gene Transfer in Neuroscience: Towards Gene Therapy of Neurologic Disorders*. John Wiley & Sons: New York, 1996, pp 263–274.
27 Halene S *et al*. Improved expression in hematopoietic and lymphoid cells in mice after transplantation of bone marrow transduced with a modified retroviral vector. *Blood* 1999; **94**: 3349–3357.
28 Shen JS *et al*. Intraventricular administration of recombinant adenovirus to neonatal twitcher mouse leads to clinico-pathological improvements. *Gene Ther* 2001; **8**: 1081–1087.
29 Glaser JH, Sly WS. Beta-glucuronidase deficiency mucopoly-saccharidosis: methods for enzymatic diagnosis. *J Lab Clin Med* 1973; **82**: 969–977.
30 Shapira E *et al*. *Biochemical Genetics: A Laboratory Manual*. Oxford University press: New York, Oxford, 1989, pp 24–35.
31 Yoshida K *et al*. Analysis of unsaturated disaccharides from glycosaminoglycuronan by high-performance liquid chromatography. *Anal Biochem* 1989; **177**: 327–332.
32 Morris R. Developments of a water-maze procedure for studying spatial learning in the rat. *J Neurosci Methods* 1984; **11**: 47–60.
33 Chang PL, Lambert DT, Pisa MA. Behavioural abnormalities in a murine model of a human lysosomal storage disease. *Neuroreport* 1993; **4**: 507–510.

[CANCER RESEARCH 64, 3545–3549, May 15, 2004]

Expression of a Novel Human Gene, *Human Wings Apart-Like (hWAPL)*, Is Associated with Cervical Carcinogenesis and Tumor Progression

Kosuke Oikawa,[1,3,4] Tetsuya Ohbayashi,[1,3,4] Tohru Kiyono,[5] Hirotaka Nishi,[2] Keiichi Isaka,[2] Akihiro Umezawa,[4,6] Masahiko Kuroda,[1,3,4] and Kiyoshi Mukai[1]

Departments of [1]Pathology and [2]Obstetrics–Gynecology, Tokyo Medical University, Shinjuku-ku, Tokyo; [3]Core Research for Evolutional Science and Technology Research Project, Japan Science and Technology Corp., Kawaguchi-shi, Saitama; [4]Shinanomachi Research Park, Keio University, Shinjuku-ku, Tokyo; [5]Division of Virology, National Cancer Center Research Institute, Chuo-ku, Tokyo; and [6]National Research Institute for Child Health and Development, Setagaya-ku, Tokyo, Japan

ABSTRACT

In *Drosophila melanogaster*, the *wings apart-like* (*wapl*) gene encodes a protein that regulates heterochromatin structure. Here, we characterize a novel human homologue of *wapl* (termed *human WAPL*; *hWAPL*). The *hWAPL* mRNA was predominantly expressed in uterine cervical cancer, with weak expression in all other normal and tumor tissues examined. hWAPL expression in benign epithelia was confined to the basal cell layers, whereas in dysplasias it increasingly appeared in more superficial cell layers and showed a significant correlation with severity of dysplasia. Diffuse hWAPL expression was found in all invasive squamous cell carcinomas examined. In addition, NIH3T3 cells overexpressing hWAPL developed into tumors on injection into nude mice. Furthermore, repression of *hWAPL* expression by RNA interference induced cell death in SiHa cells. These results demonstrate that hWAPL is associated with cell growth, and the *hWAPL* expression may play a significant role in cervical carcinogenesis and tumor progression.

INTRODUCTION

The *wings apart-like* (*wapl*) gene of *Drosophila melanogaster* encodes a protein that regulates heterochromatin structure (1). Mutations of *wapl* prevent the normal close apposition of sister chromatids in heterochromatin regions but do not appear to affect either heterochromatin condensation or chromosomal segregation (1). This evidence suggests that *wapl* is required to hold sister chromatids together in mitotic heterochromatin. *wapl* has also been implicated in both heterochromatin pairing during female meiosis and the modulation of position effect variegation (1). In addition, a *P* element screen of *Drosophila* identified *wapl* as a modifier of chromosome inheritance (2).

Among all varieties of cancer, uterine cervical cancer is unique because of its association with high-risk human papillomavirus (HPV) infection, with strains like HPV-16 and HPV-18. High-risk HPVs encode two oncoproteins, E6 and E7, which subvert crucial cellular regulatory mechanisms that reactivate and maintain DNA synthesis in the host cell. E6 accelerates proteosomal degradation of the p53 tumor suppressor, and E7 inactivates the retinoblastoma protein, interfering with the action of both $p16^{INK4a}$ (3) and the cyclin-dependent kinase inhibitor $p21^{Cip1}$ (4, 5). Both the E6 and E7 high-risk HPV oncoproteins independently induce genomic instability in normal human cells (6, 7). Only a small portion of precursor lesions infected with HPV, however, develops into invasive carcinomas (8). Therefore, additional genetic and microenvironmental factors subsequent to HPV infection are thought to play an important role in the initiation and progression of cervical neoplasia (8–10).

In this study, we describe the isolation and characterization of a novel human *wapl*-related gene termed *human WAPL* (*hWAPL*). We have also demonstrated that *hWAPL* has the characteristics of an oncogene and is associated with uterine cervical cancer.

MATERIALS AND METHODS

cDNA Cloning and Construction of the hWAPL Expression Vector. To isolate the complete *hWAPL* cDNA sequence, we used a human testis Marathon-Ready cDNA kit (Clontech, Palo Alto, CA).

To create an expression vector encoding *hWAPL*, a *Hin*dIII-*Eco*RI cDNA fragment containing the complete coding region of hWAPL was amplified by PCR using the primers 5′-TTAAGCTTTGAAACTGGTGTCAAAATGACATCCAGATT-3′ and 5′-TTGAATTCAAGCAATGTTCCAAATATTCAATCACTCTAGAG-3′ and inserted into the hemagglutinin (HA)-tagged mammalian expression vector, pHM6 (HA-hWAPL; Roche Diagnostics, Mannheim, Germany).

Northern Blot and Quantitative Real-Time PCR Analysis. RNA isolation (11) and Northern blot analysis (11, 12) were performed as described. The 674-bp *Dpn*II fragment of *hWAPL* cDNA was used as a probe and labeled with ^{32}P using the Rediprime II random prime labeling system (Amersham Biosciences, Piscataway, NJ). A human β-actin cDNA control probe (Clontech) was used as a control.

First-strand cDNA synthesis was performed as described (13). Real-time PCR analysis was performed using the Smart Cycler System (Cepheid, Sunnyvale, CA) with SYBR Green I (Cambrex, Washington, DC). Real-time PCR used the *hWAPL*-specific primers 5′-GAATTCATAGGCACAGCGCTGAACTGTGTG-3′ and 5′-TTGAATTCCTAGCAATGTTCCAAATATTCA-3′ and β-actin-specific primers 5′-GGGAAATCGTGCGTGACATTAAG-3′ and 5′-TGTGTTGGCGTACAGGTCTTTG-3′. Reaction mixtures were denatured at 95°C for 30 s and then were subjected to 40 PCR cycles at 95°C for 3 s, 68°C for 30 s, and 87°C for 6 s. *hWAPL* mRNA levels were normalized to β-actin signals.

Immunohistochemistry and Immunoblot Analysis. To generate mouse monoclonal antibodies against hWAPL, we immunized mice against a 6 × histidine-tagged hWAPL COOH terminus (amino acids 814-1037) fusion protein. Spleen cells of an immunized mouse were fused with P3UI mouse myeloma cells as described previously (14). Of the 128 hybrids generated, one clone (clone R929) showed exclusive reactivity with hWAPL by ELISA. We used the supernatant of this clone as anti-hWAPL antibody.

Immunohistochemical assays were performed on formalin-fixed, paraffin-embedded sections using Ventana HX System Benchmark (Ventana Medical Systems Inc., Tucson, AZ). Immunohistochemical stains for hWAPL were interpreted semiquantitatively by assessing the intensity and extent of staining on the entire tissue sections present on the slides as described (9).

Immunoblot analyses were performed as described previously (15). The anti-HA (Roche Diagnostics; 3F10) and monoclonal anti-α-tubulin clone B-5-1-2 (Sigma Chemical Co., St. Louis, MO; T-5168) antibodies were purchased.

Animals and Treatment. BALB/cAJcl-nu female mice (4 weeks old) were purchased from Charles River Japan, Inc. (Kanagawa, Japan).

The tumorigeneicity of the stable NIH3T3 transformants overexpressing hWAPL *in vivo* was examined as described previously (16).

Cell Culture and small interfering RNA (siRNA) Transfection. SiHa and NIH3T3 cells were grown in DMEM (Sigma) containing 10% fetal bovine serum at 37°C in a 5% CO_2 environment. For the transfection of siRNA, we

Received 12/8/03; revised 3/15/04; accepted 3/16/04.

Grant support: Grant-in-Aid for Scientific Research on Priority Area (C) and Grant-in-Aid for Encouragement of Young Scientists from the Ministry of Education, Culture, Sports, Science and Technology, Japan, and a grant from Core Research for Evolutional Science and Technology, Japan Science and Technology Corp.

The costs of publication of this article were defrayed in part by the payment of page charges. This article must therefore be hereby marked *advertisement* in accordance with 18 U.S.C. Section 1734 solely to indicate this fact.

Note: T. Ohbayashi is currently at the Horizontal Medical Research Organization, Kyoto University Faculty of Medicine, Kyoto, Japan.

Requests for reprints: Masahiko Kuroda, Department of Pathology, Tokyo Medical University, 6-1-1, Shinjuku, Shinjuku-ku, Tokyo, 160-8402, Japan. Fax: 81-3-3352-6335; E-mail: kuroda@tokyo-med.ac.jp.

generated siRNAs using a Silencer siRNA Construction Kit (Ambion, Austin, TX). siRNA transfection was performed in DMEM without serum using Oligofectamine Reagent (Invitrogen Japan, Tokyo, Japan) and Opti-MEM I (Invitrogen Japan).

For cell quantitation, we harvested the cells from the wells of a 12-well plate and resuspended them in 100 μl of PBS. Trypan blue solution (100 μl, 0.4%; Sigma) was added to each sample, and viable cell numbers were quantitated using an erythrometer. The results shown are representative of three independent cell count analyses.

RESULTS

Molecular Cloning of *hWAPL*. To isolate *wapl*-related genes from human cells, we searched DNA databases and identified a cDNA fragment, KIAA0261 (17), and three expressed sequence tag clones, BE410177, BF79516, and BE257022, containing the KIAA0261 sequence. We also performed 5′ rapid amplification of cDNA ends. From these DNA sequences, we cloned and confirmed the full-length coding region sequence of the cDNA containing KIAA0261. We named this gene *hWAPL* (GenBank accession no. AB065003) to reflect its homology to *wapl*. The *hWAPL* gene product shows high sequence similarity in the WAPL-conserved region (amino acids 627-1169, 34% identical and 56% similar) and low similarity throughout the other regions to the *wapl* gene product. Several additional stretches of amino acids are also present in wapl protein (Fig. 1*A*).

High-Level Expression of hWAPL in Human Cervical Cancer. As *wapl* is involved in sister chromatid cohesion, hWAPL may modify chromosomal inheritance. Deregulation of the expression of genes involved in chromosomal inheritance directly induces a variety of disorders associated with aneuploidy, including birth defects and cancer. Northern blot analysis detected *hWAPL* mRNA expression in several invasive cervical cancer samples, examined in tandem with additional human cancers and normal tissues (Fig. 1*B*). We confirmed the *hWAPL* expression in cervical cancers by quantitative real-time PCR analysis of tumor and normal tissue samples. The levels of *hWAPL* mRNA expression in cervical cancers were significantly higher than the levels observed in either normal cervical controls or endometrial, ovarian, breast, lung, stomach, renal, and colon cancers (Fig. 1*C*).

To investigate the connection between hWAPL expression and oncogenesis in cervical malignancies, we examined the expression of hWAPL by immunohistochemistry in a series of clinical samples of the various grades of cervical dysplasia [cervical intraepithelial neoplasia (CIN) I–III] and invasive squamous cell carcinoma. We found nuclear immunostaining for hWAPL in all samples (Fig. 2*A*). hWAPL expression in benign squamous epithelia was confined to the basal and parabasal cell layers. In contrast, hWAPL expression in squamous dysplasia and invasive carcinoma increasingly appeared in the more superficial cell layers and was significantly increased compared with the adjacent benign epithelia ($P = 0.0002$ for CIN I, $P = 0.0003$ for CIN II, $P = 0.0001$ for CIN III, and $P = 0.0001$ for invasive squamous cell carcinoma; Wilcoxon's signed rank test). CIN I and II cases showed hWAPL expression in the basal 50 and 70% of the epithelial thickness, respectively, whereas CIN III and invasive squamous cell carcinoma showed hWAPL expression in the full thickness of the dysplastic epithelia (Fig. 2*A*). Furthermore, the mean hWAPL staining score increased remarkably with increasing grade of dysplasia (Fig. 2*B*). These data strongly suggest that the unscheduled high-level expression of hWAPL may play a significant role in cervical carcinogenesis and tumor progression.

hWAPL Has Oncogenic Characteristics. Because we observed high-level expression of *hWAPL* in tumors, we sought to determine whether hWAPL overexpression promotes tumor development. We transfected NIH3T3 cells with an HA-tagged hWAPL expression vector (HA-hWAPL 3T3) or HA expression vector (HA-3T3). Then, we compared the ability of HA-hWAPL 3T3 with HA-3T3 cells to grow as tumors in nude mice. We injected 10^6 cells into three s.c. sites of each nude mouse. HA-hWAPL 3T3 cells produced tumors in all nude mice within 10 days after injection of cells (100%, $n = 18$; Fig. 3*A*). HA-3T3 failed to produce tumors in any mice (0%, $n = 18$). We confirmed high hWAPL expression levels in the resultant tumors by Western blot analysis (Fig. 3*B*). These results suggest that *hWAPL* has the characteristics of an oncogene.

Repression of hWAPL Expression Induces Cell Death. We examined hWAPL function by suppressing hWAPL expression. Initial attempts to generate a *WAPL*-deficient mouse demonstrated that the loss of *WAPL* was embryonic lethal (data not shown). Therefore, we designed two 21-nucleotide, double-stranded siRNAs, siRNA(I) and siRNA(II), to repress *hWAPL* expression (Refs. 18 and 19; Figs. 1*A*

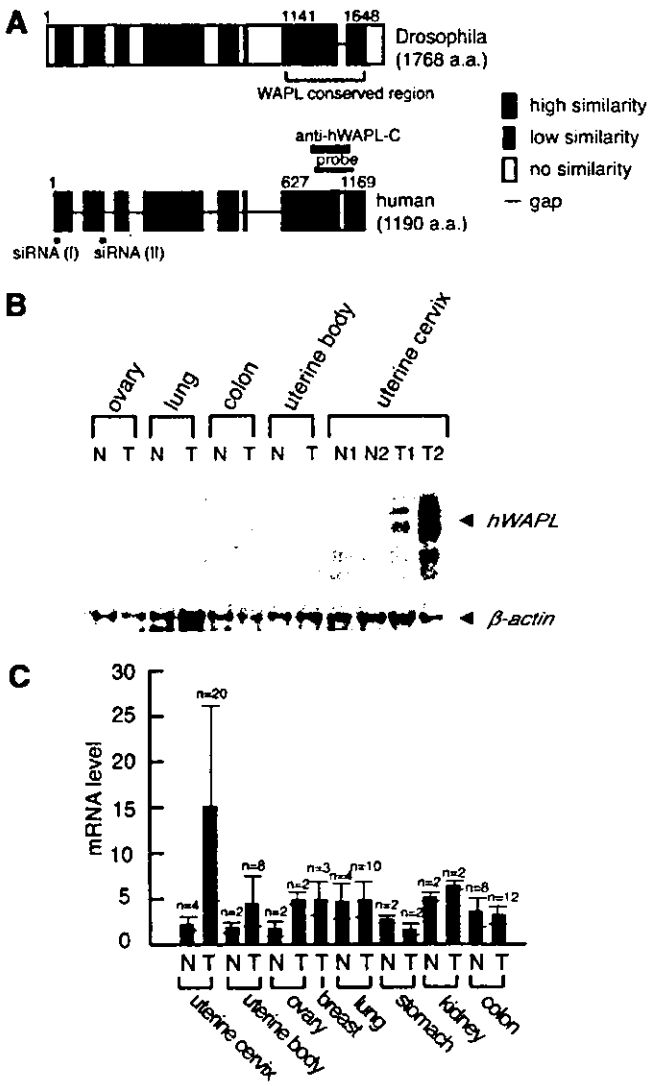

Fig. 1. Structures of wings apart-like (*WAPL*) proteins and *human WAPL* (*hWAPL*) expression in normal and tumor human tissues. *A*, schematic structure of the *hWAPL* and *Drosophila wapl* gene products. The site corresponding to the probe sequence used for Northern blot analysis is indicated by "probe." The antibody recognition site is indicated by "hWAPL-C." The small interfering RNA (*siRNA*) targeting sites are indicated by "siRNA(I)" and "siRNA(II)." *B*, Northern blot analysis of *hWAPL* in several normal (*N*) and tumor (*T*) human tissues. *C*, quantitative real-time PCR analysis demonstrating *hWAPL* mRNA levels in various normal (*N*) and tumor (*T*) human tissues. *Columns*, the means of examined samples. The minimum mRNA expression level was arbitrarily set to 1 in the graphical presentation; all other mRNA signals were normalized to this value. *Bars*, SD.

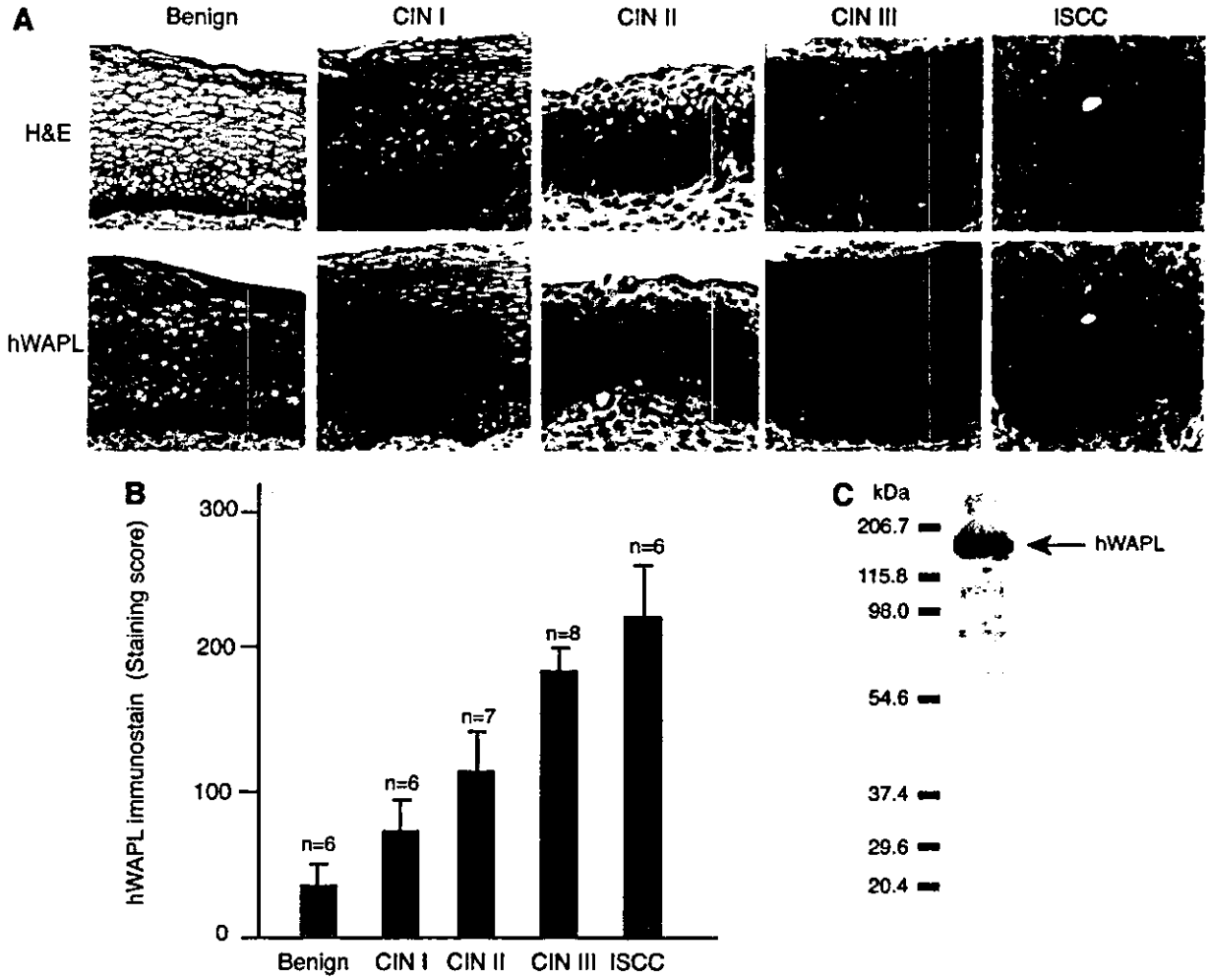

Fig. 2. Immunohistochemical analysis of human wings apart-like (*hWAPL*) expression in uterine cervical epithelia of normal, dysplasia, and carcinoma. *A*, immunohistochemical staining of hWAPL expression in benign squamous epithelium, various grades of squamous dysplasia [cervical intraepithelial neoplasia (*CIN*) grades I, II, and III], and invasive squamous cell carcinoma (*ISCC*). hWAPL was stained with hematoxylin counterstain; H&E. *B*, graphical representation of the increase of the hWAPL expression with increasing severity of dysplasia in cervical squamous epithelia. The mean hWAPL staining scores were calculated as described (9). *Bars*, SD. *C*, Western blot analysis with the total extract from a uterine cervical cancer-derived cell line, SiHa, to confirm the specificity of the anti-hWAPL monoclonal antibody hWAPL-C.

and 4*A*). We examined various human cancer-derived cell lines and found that cervical cancer-derived cell lines containing both HPV-positive and -negative cells exhibited higher levels of hWAPL expression compared with the other cell lines (data not shown). Then, we examined the effects of suppressing *hWAPL* in a cervical cancer-derived cell line, SiHa. siRNA transfection at a concentration of either 1 nM siRNA(I) or siRNA(II) reduced *hWAPL* mRNA levels (Fig. 4*B*). siRNA(I) was more effective at reducing *hWAPL* mRNA than siRNA(II). Thus, we used siRNA(I) in the subsequent experiments. hWAPL protein levels were also significantly reduced after siRNA(I) transfection (Fig. 4*C*). Interestingly, siRNA(I) repressed the growth of the cells and subsequently induced cell death (Fig. 4, *D* and *E*). siRNA(II) repressed cell growth in a similar manner as siRNA(I) (Fig. 4*D*), suggesting that the effects of these siRNAs on proliferation and viability are likely caused by the repression of *hWAPL* expression. Similar results were obtained in another cervical cancer-derived cell line, CaSki, with 10 nM siRNA(I) (data not shown). On the contrary, we did not observe any effects of siRNA(I) on cells expressing relatively low levels of *hWAPL*, such as Saos-2 and HCT116 (data not shown).

To investigate the fate of cells transfected with siRNA(I), we analyzed siRNA-transfected cells by flow cytometry (Fig. 5). In siRNA(I)-transfected cells, the population of cells exhibiting S phase DNA content increased (Fig. 5; 48 and 72 h). In addition, there was an increase in the number of apoptotic cells exhibiting subG$_1$ DNA content (Fig. 5; 72 h). Many cells showing S phase DNA content may also be apoptotic cells at G$_2$-M phase. Taken together, these results suggest that a malfunction in the hWAPL pathway activates an S phase checkpoint or another apoptotic pathway and consequently leads to cell death.

DISCUSSION

In this study, we report the isolation and characterization of a novel human gene termed *hWAPL*. We were unable to identify additional genes similar to *wapl* within the human genome sequence database. Thus, although the high-sequence conservation between hWAPL and wapl is limited to a third of the protein sequence encoded by *wapl* (Fig. 1*A*), we consider hWAPL to be the human homologue of wapl. We did not find any protein sequence motifs in hWAPL, except for the WAPL-conserved region (Fig. 1*A*). We therefore expect that hWAPL has similar functions to the wapl protein. Two hybridization signals for *hWAPL* were visible by Northern blot analysis (Fig. 1*B*). Western blot analysis, however, detected only a single band for

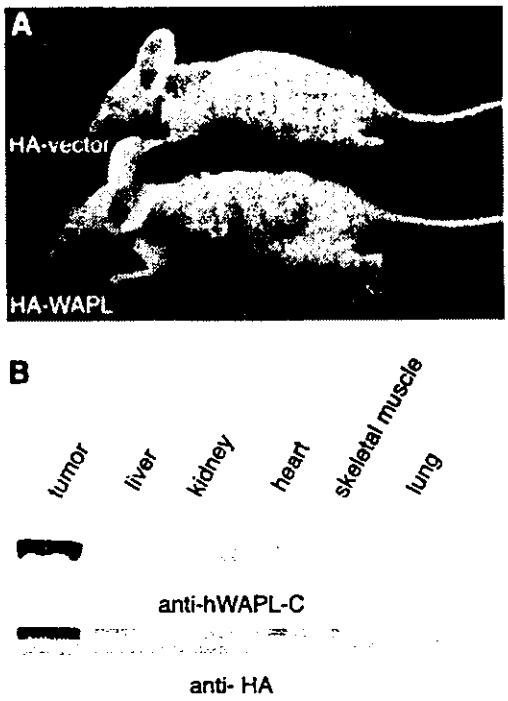

Fig. 3. Human wings apart-like (*hWAPL*) overexpression promotes tumor development. *A*, tumorigenecity of HA-hWAPL 3T3 in nude mice. The lower mouse in the *panel* is shown 10 days after the injection of HA-hWAPL-3T3 at three s.c. sites. The upper mouse was injected with the control HA-3T3 cells. *B*, Western blot analysis of hWAPL protein in tumor and other control tissues from HA-hWAPL-3T3-injected nude mice. *Top panel*, anti-hWAPL antibody; *bottom panel*, anti-HA antibody.

hWAPL (Fig. 2*C*). In addition, we did not obtain additional nucleotide sequences similar to the open reading frame of *hWAPL* by PCR analysis with various PCR primers (data not shown). Thus, we consider that the two hybridization signals may reflect the difference of the length of the untranslated regions of the *hWAPL* mRNA.

High-level expression of *hWAPL* was observed in cervical cancers (Fig. 1, *B* and *C*). Furthermore, hWAPL-overexpressing 3T3 cells developed into tumors on injection into nude mice (Fig. 3). These results suggest that *hWAPL* has oncogenic characteristics. Cervical cancer is a serious health problem, with ~500,000 women developing the disease each year worldwide. In many developing countries, it is the most common cause of cancer death and years of life lost because of cancer (20). Although the fundamental role of high-risk HPV infection in the pathogenesis of cervical carcinoma is well established, other factors are thought to play a role in cervical carcinogenesis (8, 21). Because all of uterine cervical samples examined were HPV positive (data not shown), it is still to be confirmed whether hWAPL expression is inducible by HPV infection. However, HPV-positive normal cervical tissue samples exhibited low hWAPL expression (Fig. 1, *B* and *C* and data not shown), and an HPV-negative, uterine cervical cancer-derived cell line, C33A, showed high hWAPL expression (data not shown). Thus, hWAPL expression is likely to be more closely related with cervical carcinogenesis than HPV infection. Recently, Acs *et al.* (9) found significant correlation among expression of Epo receptor, $p16^{INK4a}$, and *bcl*-2 in benign and dysplastic squamous epithelia. In our results, hWAPL showed similar expression pattern to Epo receptor and $p16^{INK4a}$ in benign and dysplastic cervical squamous epithelia and invasive squamous cell carcinomas (Fig. 2, *A* and *B*). Although we did not find any evidence for hWAPL being involved in hypoxia-inducible Epo signaling, hWAPL may cooperate with the Epo signaling in the progression of cervical neoplasia. These observations indicate that hWAPL overexpression can be used as a useful diagnostic tool in the detection of cervical dysplasia like $p16^{INK4a}$ (22) and Epo receptor (9). In addition, our results provide the necessity to investigate the potential of hWAPL as a cancer therapeutic target.

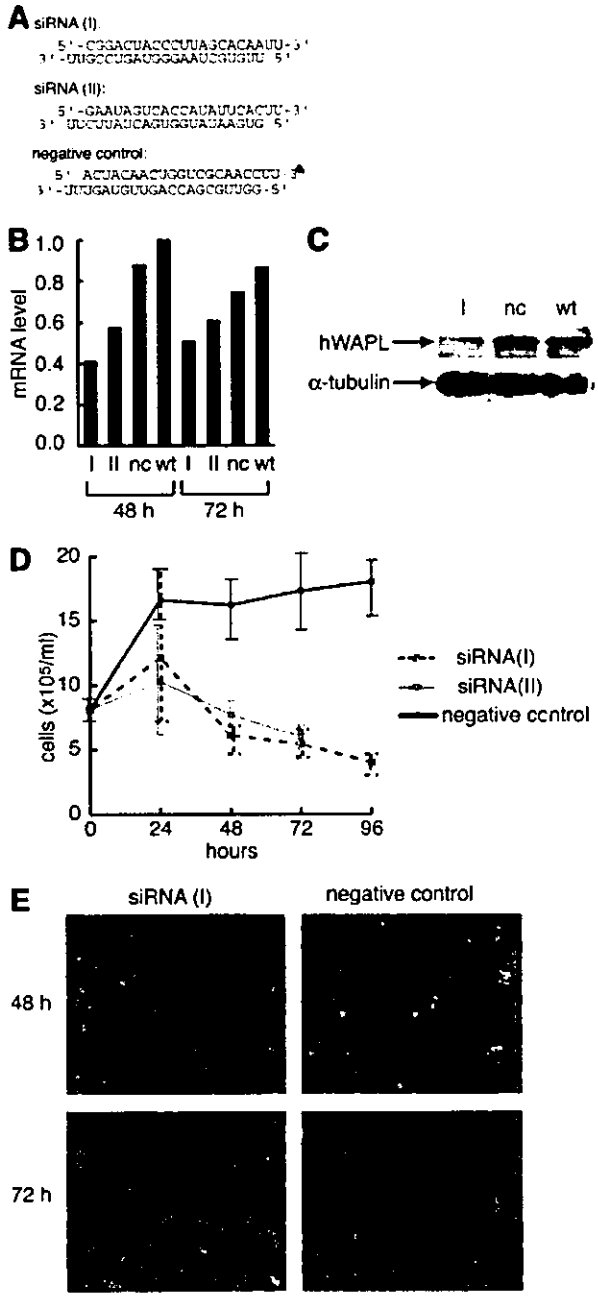

Fig. 4. Repression of human wings apart-like (*hWAPL*) expression by small interfering RNA (*siRNA*) treatment induces cell death. *A*, sequences and structures of siRNAs. The negative control siRNA possesses the same nucleotide composition as siRNA(I) but lacks homology to any known human genes. *B*, reduction of the *hWAPL* transcript by siRNA in SiHa cells. After siRNA transfection, SiHa cells were harvested at either 48 or 72 h. Total RNA was extracted from the cells and subjected to real-time PCR analysis. *I*, siRNA(I); *II*, siRNA(II); *nc*, negative control siRNA; *wt*, untransfected wild type. Data were normalized to a maximum mRNA level that was arbitrarily set to 1 in the graphical presentation. *C*, reduction of hWAPL protein levels by siRNA. Western blot analysis of total cell extracts from untreated SiHa or SiHa cells 72 h after transfection with siRNA(I) or negative control siRNA. α-tubulin is shown as a loading control. *D*, active siRNA specific for *hWAPL* induces cell death. SiHa cells transfected with siRNA(I), siRNA(II), or negative control siRNA were harvested at 24, 48, 72, and 96 h after transfection. Cell numbers were counted using an erythrometer. *Bars*, SE. *E*, representative phase-contrast images of SiHa cells transfected with siRNA(I) and negative control siRNA are shown.

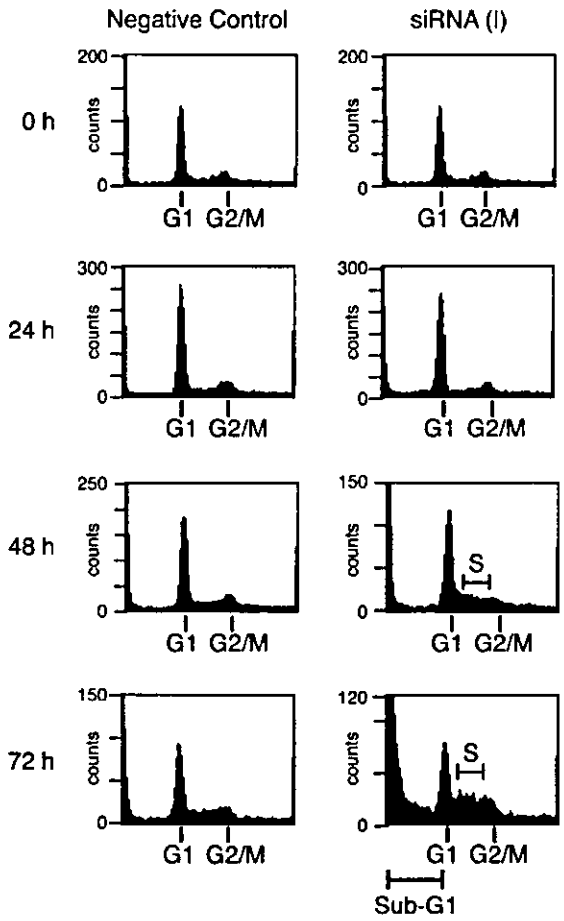

Fig. 5. Flow cytometric analysis of SiHa cells after small interfering RNA (*siRNA*) transfection. SiHa cells were transfected with either siRNA(I) or negative control siRNA, then harvested at 24, 48, and 72 h after transfection. Cells were stained with propidium iodide and subjected to flow cytometric analysis to examine DNA content. A total of 50,000 cells was counted for the sample siRNA(I) 72 h, and 20,000 cells were counted for the other samples.

Loss of WAPL was embryonic lethal in mouse (data not shown), and repression of hWAPL expression in SiHa cells led to cell death (Fig. 4). Flow cytometry analysis demonstrated that malfunction of hWAPL may cause apoptosis and/or arrest of cells at S phase (Fig. 5). In addition, *Drosophila wapl* is associated with regulation of chromatin organization (1). Thus, we expect that hWAPL is also associated with regulation of chromatin structure, and deregulation of hWAPL expression may induce chromosomal instability. Although additional investigations are necessary to elucidate the actual function of hWAPL in normal and malignant cells, our results have demonstrated that the novel oncogene, *hWAPL*, is one of the essential genes for development and cell growth and may play a significant role for cervical carcionogenesis and tumor progression.

ACKNOWLEDGMENTS

We thank K. Yoshida, R. Iwata, R. Tsujimoto, K. Kitamura, M. Sugiura, and M. Takaoka for their technical assistance.

REFERENCES

1. Verni F, Gandhi R, Goldberg ML, Gatti M. Genetic and molecular analysis of wings apart-like (wapl), a gene controlling heterochromatin organization in Drosophila melanogaster. Genetics 2000;154:1693–710.
2. Dobie KW, Kennedy CD, Velasco VM, et al. Identification of chromosome inheritance modifiers in Drosophila melanogaster. Genetics 2001;157:1623–37.
3. Kiyono T, Foster SA, Koop JI, McDougall JK, Galloway DA, Klingelhutz AJ. Both Rb/p16^{INK4a} inactivation and telomerase activity are required to immortalize human epithelial cells. Nature 1998;396:84–8.
4. Jones DL, Alani RM, Munger K. The human papillomavirus E7 oncoprotein can uncouple cellular differentiation and proliferation in human keratinocytes by abrogating p21^{Cip1}-mediated inhibition of cdk2. Genes Dev 1997;11:2101–11.
5. zur Hausen H. Papillomavirus infections–a major cause of human cancers. Biochim Biophys Acta 1996;1288:F55–78.
6. Hashida T, Yasumoto S. Induction of chromosome abnormalities in mouse and human epidermal keratinocytes by the human papillomavirus type 16 E7 oncogene. J Gen Virol 1991;72:1569–77.
7. White AE, Livanos EM, Tlsty TD. Differential disruption of genomic integrity and cell cycle regulation in normal human fibroblasts by the HPV oncoproteins. Genes Dev 1994;8:666–77.
8. Milde-Langosch K, Riethdorf S, Loning T. Association of human papillomavirus infection with carcinoma of the cervix uteri and its precursor lesions: theoretical and practical implications. Virchows Arch 2000;437:227–33.
9. Acs G, Zhang PJ, McGrath CM, et al. Hypoxia-inducible erythropoietin signaling in squamous dysplasia and squamous cell carcinoma of the uterine cervix and its potential role in cervical carcinogenesis and tumor progression. Am J Pathol 2003; 162:1789–806.
10. Schiffman MH, Brinton LA. The epidemiology of cervical carcinogenesis. Cancer 1995;76:1888–901.
11. Oikawa K, Ohbayashi T, Mimura J, et al. Dioxin suppresses the checkpoint protein, MAD2, by an aryl hydrocarbon receptor-independent pathway. Cancer Res 2001;61: 5707–9.
12. Sok J, Wang XZ, Batchvarova N, Kuroda M, Harding H, Ron D. CHOP-dependent stress-inducible expression of a novel form of carbonic anhydrase VI. Mol Cell Biol 1999;19:495–504.
13. Kuroda M, Ishida T, Takanashi M, Satoh M, Machinami R, Watanabe T. Oncogenic transformation and inhibition of adipocytic conversion of preadipocytes by TLS/FUS-CHOP type II chimeric protein. Am J Pathol 1997;151:735–44.
14. Kuroda M, Horiuchi H, Ono A, Kawakita M, Oka T, Machinami R. Immunohistochemical study on the distribution of sarcoplasmic reticulum calcium ATPase in various human tissues using novel monoclonal antibodies. Virchows Arch A Pathol Anat Histopathol 1992;421:527–32.
15. Oikawa K, Ohbayashi T, Mimura J, et al. Dioxin stimulates synthesis and secretion of IgE-dependent histamine-releasing factor. Biochem Biophys Res Commun 2002; 290:984–7.
16. Kuroda M, Wang X, Sok J, et al. Induction of a secreted protein by the myxoid liposarcoma oncogene. Proc Natl Acad Sci USA 1999;96:5025–30.
17. Nagase T, Seki N, Ishikawa K, et al. Prediction of the coding sequences of unidentified human genes. VI. The coding sequences of 80 new genes (KIAA0201-KIAA0280) deduced by analysis of cDNA clones from cell line KG-1 and brain. DNA Res 1996;3:321–9, 41–54.
18. Hannon GJ. RNA interference. Nature 2002;418:244–51.
19. McManus MT, Sharp PA. Gene silencing in mammals by small interfering RNAs. Nat Rev Genet 2002;3:737–47.
20. Waggoner SE. Cervical cancer. Lancet 2003;361:2217–25.
21. Park TW, Fujiwara H, Wright TC. Molecular biology of cervical cancer and its precursors. Cancer 1995;76:1902–13.
22. Klaes R, Friedrich T, Spitkovsky D, et al. Overexpression of p16^{INK4a} as a specific marker for dysplastic and neoplastic epithelial cells of the cervix uteri. Int J Cancer 2001;92:276–84.

THE JOURNAL OF GENE MEDICINE
J Gene Med 2004; 6: 833–845.
Published online 30 March 2004 in Wiley InterScience (www.interscience.wiley.com). DOI: 10.1002/jgm.583

RESEARCH ARTICLE

Can the life span of human marrow stromal cells be prolonged by bmi-1, E6, E7, and/or telomerase without affecting cardiomyogenic differentiation?

Yukiji Takeda,[1,2,3] Taisuke Mori,[1,2] Hideaki Imabayashi,[1,4] Tohru Kiyono,[5] Satoshi Gojo,[6] Shunichirou Miyoshi,[7] Naoko Hida,[1,2] Makoto Ita,[8] Kaoru Segawa,[9] Satoshi Ogawa,[7] Michiie Sakamoto,[2] Shinobu Nakamura,[3] Akihiro Umezawa[1]*

[1]*Department of Reproductive Biology and Pathology, National Research Institute for Child Health and Development, Tokyo, Japan;* [2]*Department of Pathology, Keio University School of Medicine, Tokyo, Japan;* [3]*Department of General Medicine and Clinical Investigation, Nara Medical University, Nara, Japan;* [4]*Department of Orthopedics, Keio University School of Medicine, Tokyo, Japan;* [5]*Virology Division, National Cancer Center Research Institute, Tokyo, Japan;* [6]*Department of Cardiovascular Surgery, Saitama Medical Center, Kawagoe, Japan;* [7]*Cardiopulmonary Division, Department of Internal Medicine, Keio University School of Medicine, Tokyo, Japan;* [8]*Pharmacia-Keio Research Laboratories, Shinanomachi Research Park, Keio University School of Medicine, Tokyo, Japan;* [9]*Department of Virology, Keio University School of Medicine, Tokyo, Japan*

*Correspondence to: Akihiro Umezawa, Department of Reproductive Biology and Pathology, National Research Institute for Child Health and Development, Okura, Setagaya, Tokyo, 157-8535 Japan. E-mail: umezawa@1985.jukuin.keio.ac.jp

Received: 23 May 2003
Revised: 16 October 2003
Accepted: 27 January 2004

Abstract

Background Cell transplantation has recently been challenged to improve cardiac function of severe heart failure. Human mesenchymal stem cells (hMSCs) are multipotent cells that can be isolated from adult marrow stroma, but because of their limited life span, it is difficult to study them further. To overcome this problem, we attempted to prolong the life span of hMSCs and investigate whether the hMSCs modified with cell-cycle-associated genes can differentiate into cardiomyocytes *in vitro*.

Methods We attempted to prolong the life span of hMSCs by infecting retrovirus encoding bmi-1, human papillomavirus E6 and E7, and/or human telomerase reverse transcriptase genes. To determine whether the hMSCs with an extended life span could differentiate into cardiomyocytes, 5-azacytidine-treated hMSCs were co-cultured with fetal cardiomyocytes *in vitro*.

Result The established hMSCs proliferated over 150 population doublings. On day 3 of co-cultivation, the hMSCs became elongated, like myotubes, began spontaneously beating, and acquired automaticity. Their rhythm clearly differed from that of the surrounding fetal mouse cardiomyocytes. The number of beating cardiomyocytes increased until 3 weeks. hMSCs clearly exhibited differentiated cardiomyocyte phenotypes *in vitro* as revealed by immunocytochemistry, RT-PCR, and action potential recording.

Conclusions The life span of hMSCs was prolonged without interfering with cardiomyogenic differentiation. hMSCs with an extended life span can be used to produce a good experimental model of cardiac cell transplantation and may serve as a highly useful cell source for cardiomyocytic transplantation.

Keywords Bmi-1; marrow stroma; cardiomyocytes; immortalization; papillomavirus; senescence

Introduction

Cell transplantation has recently been attempted to improve cardiac function in severe heart failure. Many types of cells, such as embryonic stem cells [1,2], fetal cardiomyocytes [3–5], myoblasts [6,7], bone marrow hematopoietic cells [8,9], and mesenchymal stem cells (MSCs) [10–12], have been transplanted to functionally restore damaged or diseased tissue in animal models, and mononuclear cells [13–16] or myoblasts [17] have been injected into ischemic hearts clinically.

MSCs can be a useful source of cells for transplantation for several reasons: they have the ability to proliferate and differentiate into mesodermal tissues, including heart, they entail no ethical or immunological problems, and bone marrow aspiration is an established routine procedure. When placed in appropriate *in vitro* and *in vivo* environments, MSCs can give rise to all major mesenchymal tissues, such as bone, cartilage, muscle, and adipose tissue [18]. Murine MSCs can also differentiate into cardiomyocytes and start to beat synchronously *in vitro* [19], and direct injection of murine MSCs into the heart has been shown to be feasible in murine models of ischemic heart disease and normal mouse heart. Thus far, only endothelial cells have been shown to exhibit '*in vitro* cardiomyogenesis' in humans [20].

Large numbers of cells must be injected into damaged sites in ischemic heart disease to restore cardiac function in humans, and cells need to be injected into the entire heart in cardiomyopathy. Until now, however, there have been no reports of a sufficient number of differentiated human cardiomyocytes ever having been obtained to restore the function of a failing heart. One of the reasons for this is that the life span of human cells *in vitro* is limited. Human cells reach senescence or stop cell growth after a limited number of cell replications [21], and the average number of hMSC population doublings (PDs) has been found to be 38 [22], implying that it would be difficult to obtain enough cells to restore the function of a failing human heart.

To resolve these problems and to establish a model of cell therapy of the failing heart, we attempted to prolong the life span of hMSCs by using the system to infect retrovirus encoding bmi-1, human telomerase reverse transcriptase (TERT), and human papillomavirus E6 and E7 genes. Both Rb/p16INK4a inactivation with E7 and telomerase activation with E6 are required to extend the life span of human epithelial cells [23]. bmi-1, a c-myc cooperating oncogene in murine lymphomas, reduces expression of p16INK4a, stimulates cell proliferation [24], and is required for maintenance of self-renewing hematopoietic stem cells [25,26]. This method was highly efficient in extending the life span of hMSCs. In the present study we investigated whether hMSCs with an extended life span have the ability to differentiate into cardiomyocytes *in vitro*.

Materials and methods

Isolation and cell culture of hMSCs

After obtaining signed informed consent, bone marrow cells were harvested from a 91-year-old human female donor with the approval of the Ethics Committee of Keio University School of Medicine (Tokyo). Cells were resuspended in bone marrow stromal cell culture medium (10% fetal bovine serum in Dulbecco's modified Eagle's medium containing 4.5 g/l glucose [DMEM-HG]) with antibiotic/antimycotic supplements (Gibco), and cultures were maintained at 37 °C in a humidified atmosphere containing 95% air and 5% CO_2. When the cultures reached subconfluence, the cells were harvested with 0.25% trypsin and 1 mM EDTA, and replated with one half of the harvested cells. After a series of passages, the attached marrow stromal cells were devoid of hematopoietic cells. Several bone marrow stromal cell strains were then generated by the limiting-dilution method, and one of them was designated H4-1. The H4-1 cells were cultured in MSC growth medium (MSCGM) at 37 °C in a humidified atmosphere containing 95% air and 5% CO_2.

Preparation and infection of recombinant retroviruses

The full-length human bmi-1 cDNA was cloned by RT-PCR using RNA extracted from K562 cells. Thermoscript reverse transcriptase (Invitrogen) and KOD polymerase (TOYOBO, Japan) were used for the RT and PCR reactions, respectively. The forward primer, 5′-ACGCGTCGACCGCCATGCATCGAACAACGAGAAT-3′, and reverse primer, 5′-CGGATCCTCAACCAGAAGAAGTTGCTG-3′, were designed to obtain the coding sequence of human bmi-1 flanked by the *Sal*I site (underlined) and the Kozak consensus sequence at the 5′-end and the *Bam*HI site (underlined) at the 3′-end. The *Sal*I-*Bam*HI segment of the PCR product was cloned between the *Xho*I and *Bgl*II sites of pCLXSN to generate pCLXSN-bmi1. The coding sequence of the cDNA was confirmed to be identical to the published sequence (NCBI ACC# NM_005 180.4). Construction of pCLXSH-hTERT has been described previously [27]. The gateway system (Invitrogen) was used to subclone a deletion mutant of HPV16 E6 (16E6SDD151) that lacked transforming activity to 3Y1 cells [28] into pCMSCVpuro. pCMSCVpuro comprises the CMV/LTR fusion promoter, the packaging signal Psi, and the multicloning sequence from pCLXSN (Imgenex Corp., San Diego, CA, USA) followed by the PGK-puro cassette and the 3′ long terminal repeat of murine embryonic stem cell virus from pMSCVpuro (Clontech). The destination vector pCMSCVpuro-DEST was constructed by inserting a modified cassette containing attR sites and ccdB (Invitrogen) between the *Eco*RI and *Bgl*II sites of pCMSCVpuro. 16E6SDD151 was first recombined into pDONR201 by BP reaction, and then into the destination vector by LR reaction according to the manufacturer's instructions (Invitrogen) to generate pCMSCVpuro-16E6SDD151. Production of recombinant retroviruses has been described previously [29,30]. Briefly, the retroviral vector together with the packaging construct, pCL-10A1, was transfected into 293T cells, and the culture fluid was harvested 48–72 h post-transfection. The preparation of the LXSN-16E7 retrovirus and the infection protocols have been described previously [31], except that FLYA13 [32] was used as the packaging cell line instead of PG13. The titers of the recombinant viruses were greater than 5×10^5 drug-resistant colony-forming units per milliliter on HeLa

cells, and 1 ml of the culture fluid was added to the cells in the presence of polybrene (8 μg/ml). Following inoculation with the viruses, hMSCs were grown in the presence of G418 (100 μg/ml), hygromycin B (50 μg/ml), or puromycin (1 μg/ml), and a polyclonal drug-resistant cell line was established and further analyzed. To achieve combinations of retroviral infections, cells were sequentially transduced with LXSN-E7 or LXSN-bmi-1, and LXSH-hTERT, and then MSCVpuro-16E6SDD151, if indicated, and selected with G418, hygromycin B, and puromycin, respectively. The stably transduced cells with an expanded life span were designated UBT-5, UBET-7, UEET-1, UEET-11, and UET-13.

Flow cytometric analysis

Cells were detached and stained for 30 min at 4 °C with primary antibodies and immunofluorescent secondary antibodies. After washing, the cells were analyzed on an EPICS ALTRA analyzer (Beckman Coulter). Antibodies (anti-human CD13, CD14, CD24, CD29, CD31, CD34, CD44, CD45, CD50, CD54, CD55, CD59, CD90, CD105, CD117, CD133, CD140a, CD166, Flk-1) were purchased from Beckman Coulter, Immunotech, Cytotech, and Pharmingen Pharmaceutical, Inc.

Introduction of the GFP and β-galactosidase genes

Recombinant adenovirus expressing β-galactosidase and the green fluorescent protein (GFP) was prepared as described [33]. Cells were infected with these viruses at 10 plaque-forming units/cell. hMSCs were examined cytochemically *in vitro* for expression of the β-galactosidase gene and by fluorescent confocal microscopy for expression of the GFP gene. By 7 days post-infection nearly all the cells expressed β-galactosidase and GFP.

Preparation of murine fetal cardiomyocytes

Fetal cardiomyocytes were obtained from the hearts of day 14 mouse fetuses. Hearts were minced with scissors and washed with phosphate-buffered saline (PBS), and the minced hearts were incubated in PBS with 0.05% trypsin and 0.25 mM EDTA for 5 min at 37 °C. After adding DMEM supplemented with 10% fetal bovine serum (FBS), the cardiomyocytes were centrifuged at 1000 rpm for 5 min. The pellet was then resuspended in 10 ml DMEM with 10% FBS and incubated on glass dishes for 1 h to separate the cardiomyocytes from fibroblasts. The floating cardiomyocytes were collected and replated at $1 \times 10^5/cm^2$.

hMSC and murine fetal cardiomyocyte co-culture system

Human MSCs were plated on dishes at $5 \times 10^4/cm^2$, and infected with EGFP-expressing adenovirus on the next day. The supernatant was then removed, and the cells were cultured for 2 days in DMEM supplemented with 10% FBS. The cells were then exposed to 10 μM of 5-azacytidine for 24 h to induce cell differentiation. The 5-azacytidine-treated hMSCs were harvested with 0.25% trypsin and 1 mM EDTA and overlaid onto the fetal cardiomyocytes at $5 \times 10^3/cm^2$. The morphology of the beating hMSCs was evaluated under a fluorescent microscope.

RT-PCR

Total RNA was prepared from co-cultured hMSCs and mouse heart with Isogen (Nippon Gene). Human cardiac RNA was purchased (Clontech). RNA for RT-PCR was converted to cDNA with a first-strand cDNA synthesis kit (Amersham Pharmacia Biotec) according to the manufacturer's recommendations. RT-PCR of the bmi-1, E6, E7, TERT, myosin light chain-2a (MLC-2a), Nkx2.5, and human atrial natriuretic peptide (hANP) genes was performed, and the PCR primers used are listed in Table 1. RT-PCR was performed with PCR primers that can amplify human but not mouse genes. PCR primers of 18S used as a positive control react with both human and murine genes. PCR was performed with TaKaRa Z-Taq (Takara Shuzo Co., Ltd) for 30 cycles, with each cycle consisting of 98 °C for 5 s, 68 °C or 60 °C for 1 s, and 72 °C for 10 s, with an additional 30-s incubation at 72 °C after completion of the final cycle.

Action potential recording and microinjection of dye

An inverted microscope (IX-70, Olympus, Tokyo, Japan) with a fluorescence filter (U-MNIBA2, Olympus) was used for action potential (AP) recording. The microscope was equipped with a recording chamber and a noise-free heating plate (Microwarm Plate, Kitazato Supply, Fujinomiya, Shizuoka, Japan). A 10 mmol/l volume of HEPES was added to the culture medium to stabilize the pH of the perfusate at 7.5–7.6. Standard glass microelectrodes having a DC resistance of 25–35 MΩ when filled with pipette solution were used. Alexa 568 compound was dissolved to a concentration of 0.5 mmol/l in 2 mol/l of KCl solution in order to completely dissolve the Alexa 568 in the pipette solution. The electrodes were positioned with a motor-driven micromanipulator (PCS-5000, Burleigh Instruments, Inc., New York, USA) under optical control. Spontaneously beating GFP-positive cells were selected as targets, and, after the APs of the targeted cells had been recorded, the dye was injected by iontophoresis (−7 nA for 30–60 s). The extent